When did the Kalahari craton form? Constraints from baddeleyite U-Pb geochronology and geo-chemistry of mafic intrusions in the Kaapvaal and Zimbabwe cratons

Nadine März

Master thesis in geology at Lund University - Lithosphere and Paleobiosphere Sciences, no. 268 (45 hskp/ECTS)

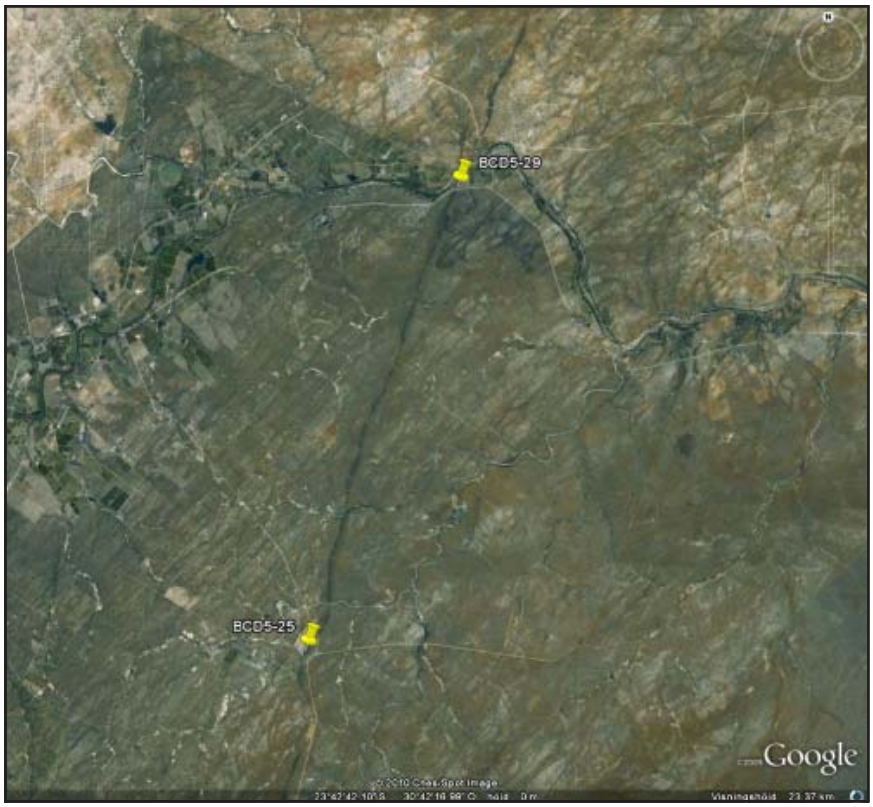

Department of Earth- and Ecosystem Sciences
Division of Geology
Lund University
2010

When did the Kalahari craton form? Constraints from baddeleyite U-Pb geochronology and geochemistry of mafic intrusions in the Kaapvaal and Zimbabwe cratons

Master Thesis

Nadine März

Department of Geology

Lund University

2010

Table of contents

Abstract

The NE-trending Black Hills dolerite dykes make up a prominent swarm northeast of the Bushveld Igneous Complex in the Kaapvaal craton. Baddeleyite U-Pb dates of five dykes suggest emplacement ages between ca. 1.87 Ga and 1.85 Ga, with two samples yielding robust ages of 1852 ± 5 Ma and 1863 ± 7 Ma. The Black Hills swarm is thus largely coeval with the post-Waterberg dolerite sills (1.88-1.87 Ga) and basalts of the Soutpansberg Group in northern Kaapvaal as well as with the extensive Mashonaland sill complex (1.89-1.86 Ga) that is abundant across Zimbabwe and Botswana. Together, these intrusions and extrusions manifest a regional-scale extensional event that is common in both the Kaapvaal and Zimbabwe cratons. Additional, younger events common in both cratons are the ca. 1.1 Ga Umkondo and ca. 0.18 Ga Karoo large igneous provinces, suggesting that the Kaapvaal and Zimbabwe cratons have been nearest neighbours from at least 1.9 Ga to present time. In contrast, not a single common event older than 1.9 Ga has been recorded suggesting that the Kalahari craton was not formed until ca. 2.0 Ga.

Recent U-Pb dating has revealed the presence of older dykes, approximately 2.7 Ga in age (Johan Olsson, unpublished data), intermixed with the ca. 1.87– 1.85 Ga dykes of the Black Hills swarm. Geochemistry of 28 dykes of the Black Hills swarms and of 2 Mashonaland sills in Zimbabwe were analysed with respect to both major and trace elements. Geochemical data indicate that each generation of dykes can be petrogenetically related. There are no significant differences between the 2.7 Ga and ca. 1.87– 1.85 Ga dykes, but more so between more evolved and primitive dykes within each group. It is possible that primary melts were generated at relatively shallow (from the spinel stability field) mantle depths and that these primary melts subsequently experienced shallow crustal fractionation of, at least, plagioclase, some Mg-rich phase(s) and apatite. Relatively high concentrations of most incompatible elements suggest that the mantle source was more enriched than a normal MORB source. Any additional enrichment in large-ionic lithophile elements and negative Nb-Ta anomalies can be ascribed to contamination and/or partial melting of the Kaapvaal craton lithosphere.

Sammanfattning

Nordost om Bushveldkomplexen i Kaapvaal kratonen finns en mäktig gångsvärm av nordost-orienterade diabasgångar tillhörande ”the Black Hills dyke swarm”. Med hjälp av U- Pb metoden av mineral baddeleyit daterades fem gångar inom ålderspannet 1.87 - 1.85 Ga, där två av dem ger exakta åldrar på 1852 ± 5 Ma och 1863 ± 7 Ma. Denna gångsvärm är alltså lika gammal som lagergångar tillhörande ”post- Waterberg sills” (1.88 - 1.87 Ga), basalter tillhörande ”Soutpansberg” i norra Kaapvaal och Mashonaland lagergångar (1.89- 1.86 Ga) i Zimbabwe och Botswana. Kaapvaal- och Zimbabwe-kratonerna har således ”minnen” av tre gemensamma och regionala magmatiska händelser vid: 1.99-1-85 Ga (ovan nämnda enheter), ca. 1.1 Ga (Umkondo) samt ca. 0.18 Ga (Karoo). Ålderspassningar äldre än 1.9 Ga förekommer däremot inte. Dessa resultat indikerar Zimbabwe och Kaapvaal tillhörde ett och samma block från 1.9 Ga till idag, och att Kalaharikratonen inte existerade förrän 2.0 Ga.

Kemidata av 28 gångar från Black Hills svärmen och från 2 Mashonaland lagergångar i Zimbabwe analyserades med avseende på huvud- och spårelement. Tidigare dateringar (Johan Olsson, in prep.) visar att vissa gångar tillhörande Black Hills svärmen är betydligt äldre, cirka 2.7 Ga, än de som daterats i dennta studie. Geokemidata för dessa olika generationer av diabas är sammantaget snarlika, vilket skulle kunna betyda att de har bildats genom uppsmältning av liknande ursprungsmaterial (mantel). Datan indikerar också att båda generationerna bildades genom uppsmältning från relativt grunda djup (spinell-förande mantel) och att de kemiska sammansättningarna pekar på fraktionering av plagioklas, Mg-rika mineral (olivin och pyroxen) och apatit. Proverna innehåller höga halter inkompatibla spårelement, och härstammar därför troligen från en mantelkälla som är mer anrikad än en MORB källa. Anrikning av LILE och negativa Nb- Ta avvikelser visar kontaminering och/eller partiell smältning av litosfärsfäriska manteln tillhörande Kaapvaalkratonen.

1. Introduction

Today, we possess new tools to solve ancient configurations of supercontinents, and constrain the geographic position of crustal blocks between supercontinent cycles. Mafic dyke swarms can reach thousands of km in length and consist of dykes with similar trends that once were emplaced in a short time interval, typically within a few Ma (Ernst et al., 1995). They represent key rocks for solving the pre-Pangean palaeogeography of crustal blocks because (1) they are frequently associated with Large Igneous Provinces (LIPs) present on all cratons worldwide (Ernst and Buchan, 2001), (2) they have the ability to record and preserve the Earth's magnetic direction at the time of their crystallisation, and (3) they often contain baddeleyite (ZrO_2) that can be precisely dated by U-Pb isotopic systematics (e.g. Heaman and LeCheminant, 1993, Söderlund et al., 2006). Ages of dyke swarms and other components of LIPs can be compiled into a magmatic barcode for each of the ca. 35 Archaean cratons worldwide (Bleeker, 2003), where each bar represents a single magmatic event. Crustal units that share several, or at least two, bars (i.e. magmatic events) can be argued to have existed as a coherent unit in a next-neighbour situation and subsequently rifted apart (Ernst et. al., 1995).

The Archaean granite-greenstone basement of the Kaapvaal and the Zimbabwe cratons are intruded by a large number of mafic dykes with Archaean to Phanerozoic ages (e.g. Hunter and Reid, 1987; Hanson et al., 2004a; Olsson et al., in press; Söderlund et al., in press). The east-northeast trending Limpopo belt manifests the collisional event between the Kaapvaal and Zimbabwe cratons as well as the formation of the Kalahari craton. The width of the belt is approximately 250 km and is made up of high-grade metamorphic rocks. The timing of this collisional event has been much debated due to the fact that radiometric dating of metamorphic minerals give ages that cluster at both 2.7 Ga and 2.0 Ga (e.g. Mouri, 2008; Eriksson et al., 2008; Zeh et al., 2010, and references therein).

East of the 2.06 Ga Bushveld Complex in the Kaapvaal craton, three major swarms with different dyke directions intrude the Archaean basement. In this study five dykes of the most northerly, NE-trending

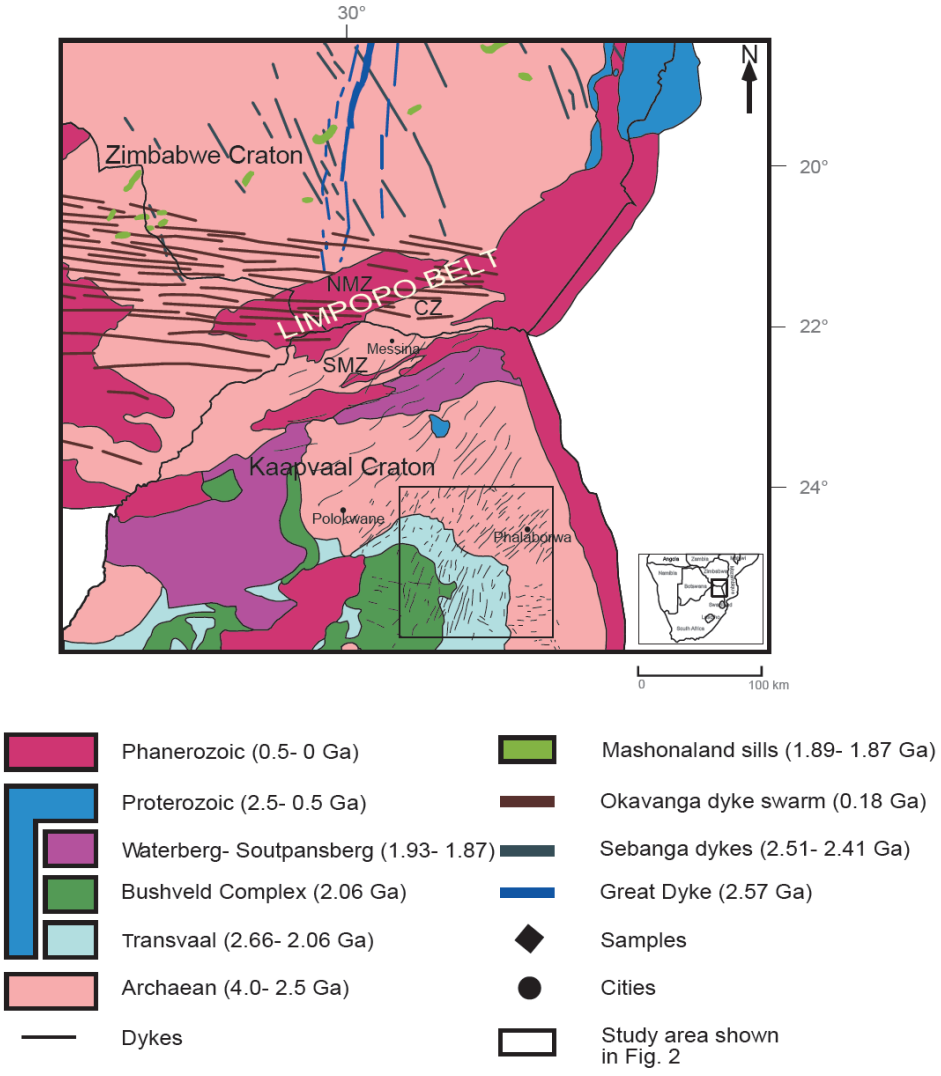

Figure 1. Simplified geological map showing the northern part of the Kaapvaal craton (modified from Johnson et al., 2006), the Limpopo belt including the Northern Marginal Zone (NMZ), the Central Zone (CZ) and the Southern Marginal Zone (SMZ) and the southern part of the Zimbabwe craton (modified from Stubbs et al., 1999 and Wilson et al.,1987).

swarm, called the Black Hills swarm, were dated using U-Pb on baddeleyite grains. On the basis of varying degree of alteration, Uken and Watkeys (1997) argued this swarm comprises at least two generations of dykes: one late Archaean and one younger suite, the latter possibly as late as Phanerozoic. Subsequent $^{40}Ar/^{39}Ar$ geochronology confirmed a complex origin for the dykes of this swarm (Jourdan et al., 2006).

The rationale of this study has been to obtain precise emplacement ages of dykes of the Black Hills swarm. If these dates can be matched with recently published ages of mafic intrusions in the Zimbabwe craton (Söderlund et al., in press), they may better constrain the timing of formation of the Kalahari craton, i.e. when these two cratons collided to form a single crustal unit.

Furthermore, 28 dykes from the Kaapvaal craton, comprising dykes for the Black Hills swarm and two samples from the Mashonaland sills in Zimbabwe (dated by Söderlund et al., in press), are geochemically described and compared to other published data on coeval magmatic events (e.g. Stubbs, 1999; Stubbs et al., 2000; Klausen et al., in press). The spatial distribution and geometry of these intrusions and lavas provide some additional constraints on the palaeo-tectonic setting, which, compared with compositional signatures, lead to petrogenetic inferences.

2. Geological setting

2.1. Kaapvaal craton and its Precambrian cover rocks

The Kaapvaal craton is dominated by Achaean granitoids, gneisses and greenstone belts, and comprises mainly northern South Africa and eastern Botswana (Fig. 1). It is one of the Earth's oldest craton, made up of rocks dating back to ~3.7 Ga (Eglington and Armstrong, 2004). The stabilisation of the entire Kaapvaal craton was completed by ~2.6 Ga (James et al., 2003). In the west, the craton is delimited by the ~2.0 Ga Kheis overthrust belt (de Wit et al., 1992), in the north by the Limpopo belt, and in the south and east by the 1.9-1.1 Ga Namaqua-Natal Proterozoic mobile belt. The eastern margin is also covered by the Jurassic Lembombo Group volcanics which erupted during the Gondwana breakup.

The Ancient Gneiss Complex, with protolith ages ranging between 3.5 and 3.6 Ga, represents the oldest part of the Kaapvaal craton. A number of greenstone belts occur of which the largest, oldest and one of the most well preserved is the 3.5-3.2 Ga Barberton Greenstone Belt (Kröner and Compston, 1988). Another well known belt is the 3.1-3.0 Ga Murchinson Greenstone Belt (Poujol et al., 1996), located in the Northern Province, representing a volcanic arc sequence.

The oldest preserved cover sequence on the Kaapvaal craton is the 3.07 Ga Dominion Group (Armstrong et al., 1991), consisting mainly of volcanic deposits.

The Pongola Supergroup with ages between ca. 2.95 and 2.85 Ga (Strik et al., 2007) is made up of a predominantly volcanic lower part (Nsuze Group) and a predominantly clastic sedimentary upper part (Mozaan Group). Together with the older Dominion Group and coeval Witwatersrand Supergroup, farther to the west, it unconformably overlies the granite-greenstone basement (Button, 1981).

The Pongola and Witwatersrand Supergroups are unconformably overlain by the Ventersdorp Supergroup (ca. 2.71-2.70 Ga), which is a highly volcanic sequence. The basal Klipriviersberg group, dated at 2714 ± 8 Ma (Armstrong et al., 1991), is characterised by subaerial flood basalts with subordinate sediments. The middle sequence of the Makwassie Formation has been dated at 2709 ± 5 Ma (Armstrong et al., 1991). The Ventersdorp Supergroup is unconformably overlain by volcanics and immature clastic sediments.

The Transvaal Supergroup preserves one of the major Archaean to Palaeoproterozoic basin sequences within the Kaapvaal craton including low-grade metasedimentary and minor metavolcanic rocks (Mapeo et al., 2006). It overlies unconformably the Ventersdorp Supergroup (Eriksson et al., 2001). Deposition of the Transvaal Supergroup took place between 2.66 Ga and 2.06 Ga (Eriksson et al., 2006). The lower Neoarchaean part of the Transvaal Supergroup is dominated by iron-rich carbonate sequences whereas its upper part is characterised mostly by siliciclastic rocks including minor volcanics.

The Transvaal Supergroup is intruded and overlain by the ca. 2.06 Ga (Buick et al., 2001; Olsson et al., in press) Bushveld complex, including the world's largest layered intrusion (Rustenburg Layered Suite), an older Rooiberg Group lava sequence, and younger Lebowa granite and Rashoop granophyre Group intrusions. The mafic-ultramafic Rustenburg Layered Suite hosts large and economically important platinum group elements, as well as chromium and vanadium deposits (Lee,1996). The large intrusion also contact-metamorphosed the Transvaal Supergroup host to variable degrees (Sharpe, 1981).

The ~1.93-1.87 Ga Waterberg Group (Hanson et al., 2004b) lies unconformably on top of both the Transvaal and the Bushveld complex. The predominantly sedimentary Waterberg Group has a stratigraphic thickness of up to 7 km and represents a Proterozoic sedimentary deposit within the continental basin in the northern part of the Kaapvaal craton (Hanson et al., 2004b).

There is some stratigraphical uncertainty regarding the correlations between the Waterberg and the Soutpansberg Group, but the Waterberg is believed to be unconformably overlain by the Soutpansberg Group (Bumby et al., 2001 and 2002). The Soutpansberg Group outcrops in the northern Kaapvaal, along the southern margin of the Limpopo Belt. It is made up of both lower volcanic and upper sedimentary rocks, which probably accumulated within an elongated continental rift basin. The NE- trending dykes of the Black Hills swarm may be feeders to the lavas of the Soutpansberg Group (Klausen et al., in press).

2.1.1. Dykes within the Kaapvaal craton

There are three major dyke swarms in the Archaean basement east of the ~2.06 Ga Bushveld Complex (Fig. 1). In the south, the 3.2–3.5 Ga Barberton Greenstone Belt and most of its surrounding granitoids are cut by many dykes (Brandl et al., 2006). The perhaps most prominent swarm is the NW-SE trend-

ing Badplaas Dyke Swarm, recently dated with an emplacement age of 2965.9 ± 0.7 Ma (Olsson et al., in press). This dyke swarm is approximately 80 km wide and 100 km long. Both high-Ti and low-Ti types of dolerite dykes can be distinguished within this swarm (Hunter and Halls, 1992). These authors noticed that the high-Ti dykes show geochemical characteristics similar to the 2984 ± 2.6 Ma lavas from the Nsuze Group whereas the low-Ti dykes show geochemical characteristics typical of early Proterozoic dykes. Other early to middle Proterozoic dykes, striking mostly ENE or NE, are intrusive into the Transvaal Supergroup and the Waterberg Group and are macroscopically similar to the undeformed Archaean dykes and also have a similar strike direction (Hunter and Reid, 1987).

North of the Badplaas Dyke swarm, a distinct E-W trending swarm was recently dated at 2.7 Ga (Olsson et al., in press). This E-W trending Rykoppies Dyke Swarm is approximately 50 km wide and 100 km long. Uken and Watkeys (1997) proposed these dykes to be feeders to the Bushveld complex and coeval sills within the Transvaal Supergroup (e.g. Sharpe, 1981) because these are orientated parallel to and extend from the east-west trending long axis of the complex. However, a ~2.7 Ga age for the dykes rather suggests a link to the Ventersdorp Supergroup.

In the north, a NE-SW trending swarm (Figs. 1 and 2), referred here to as the Black Hills swarm, extends from the Archaean basement into the 2.66-2.06 Ga Transvaal Supergroup (Eriksson et al., 2006) and the ~2.06 Ga Bushveld Complex (Cawthorn et al., 2006). Uken and Watkeys (1997) subdivided this swarm into two groups; (1) more altered, so called diabase, dykes in the northern part, and (2) less altered, so called dolerite, dykes in the south (this division assumed that dolerite dykes were related to the 0.18 Ga Karoo event and Gondwana break up). However, dykes of the Black Hills swarm yielded $^{40}Ar/^{39}Ar$-ages from 0.7 to 1.7 Ga and from 2.5 to 2.9 Ga (Jourdan et al., 2006), but these numbers can only be taken as rough age estimates. At the margin to the Transvaal Supergroup the overall dyke direction switches rather abruptly from NE to NNE (Fig. 2), possibly indicating two separate generations of dykes or an original or secondary regional change in the trend of a single swarm. Letts et al. (2005) reported an $^{40}Ar/^{39}Ar$ age of 1649 ± 10 Ma for dykes intruding the Bushveld complex, which these authors discussed to represent cooling or thermal disturbance. ENE-trending dykes near Messina (Fig. 1) were dated at ~2.2 Ga using Rb-Sr (Barton, 1979) and ~1.5-1.8 Ga (Jacobsen et al., 1975), the latter which may correlate with the 1.87– 1.85 Ga dykes of the Black Hills swarm further to the south (Hunter and Reid, 1987). Unless isotopically disturbed the 2.2 Ga Rb-Sr age of Barton (1979) could temporally be linked with the accumulation of some isolated mafic volcanics (Hekpoort Formation) within the Transvaal Basin (Eriksson et al, 2006). The 1.9 Ga dyke event could be related to the

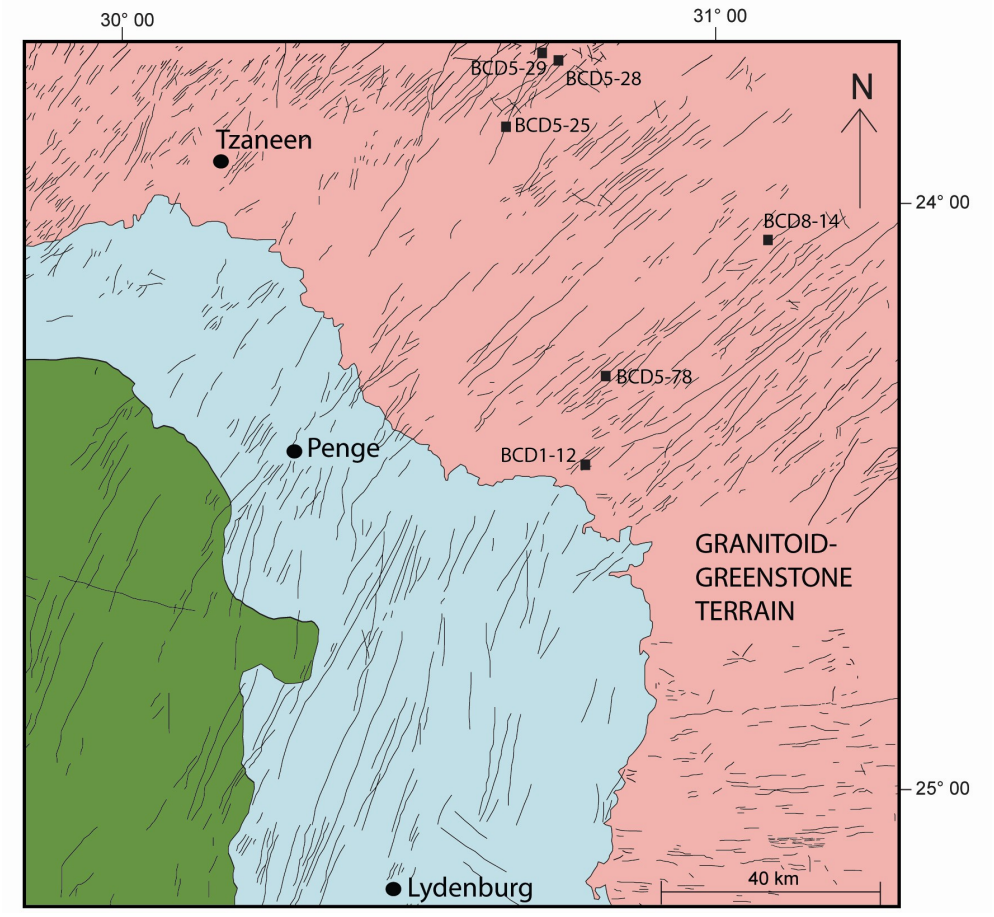

Figure 2. Geological map showing the distribution of dolerite dykes in the Eastern Kaapvaal (Modified from Uken and Watkeys, 1997). Dyke sampled for geochronology are marked with sample name. Map colours as in Fig. 1.

same rifting event that gave rise to the initiation of the Waterberg basin and subsequent deposition of Soutpansberg lavas (Hunter and Reid, 1987). The widespread dolerite sills that intrude the Waterberg Group and predate the Jurassic Karoo magmatism are called "Post-Waterberg dolerites" with ages from ~1.88 to ~1.87 Ga (Hanson et al., 2004b). Another dyke swarm is intrusive into the Waterberg Group in the north central part of the Kaapvaal craton. The NW- trend of these dykes is coincident with that of major faults in the northern-central Kaapvaal province (Hunter and Reid, 1987).

2.2. Zimbabwe Craton

The Archaean Zimbabwe craton borders the Limpopo belt in the south and the Pan-African Mozambique and Zambezi mobile belts in the east and north, respectively. It is overlain partly by Palaeoproterozoic to Phanerozoic rocks (Fig. 1). This craton consists of granite-greenstone terranes formed during two stages of crust generation (Luais and Hawkesworth, 1994). During the 1st stage (3.5 -3.3 Ga), undeformed and deformed granitoids and granitoid gneisses were formed in the south of the craton. The 2nd stage (3.0-2.6 Ga) is associated with formation of greenstone belts made up of volcanics, volcanoclastics and epiclastic rocks, banded-iron formations (BIFs), and ultramafic intrusions, which were all affected by low grade metamorphism. There are three main greenstone sequences on the Zimbabwe craton. The oldest is the ~3.5 Ga Sebakwian Group, which is represented by remnants of greenstones that are infolded with gneisses. They contain quartz-magnetite BIFs and some diopside quartzites (Wilson et al., 1995). Metamorphism up to amphibolite and greenschist facies affected these rocks. Stratigraphically younger is the ~2.9 Ga Belingwean Supergroup (Wilson et al., 1995), made up of mafic and ultramafic lavas and intrusions overlain by sediments (Nisbet et al., 1977). It is divided into a lower and upper group (Poujol et al., 1996), which both consist of mafic volcanic sequences but include more BIFs in the upper sequence. The youngest greenstone sequence is the Bulawayan Supergroup (2.7 Ga), which is also subdivided into a lower and an unconformably overlying upper group (Wilson et al., 1995). The lower group is made up of felsic and dacitic flows, andesites and volcanoclastic sediments whereas the upper group is made up of komatiites, komatiitic basalts, tholeiites and associated sediments. Approximately 2.6 Ga old granite intrusions mark the final crustal-building phase and stabilisation of the Zimbabwe craton.

2.2.1. Dykes and sill complexes within the Zimbabwe craton

The Zimbabwe craton hosts a number of mafic dykes ranging in age between 2.7 and 0.18 Ga (Fig. 1), the younger generation corresponding to the ca. 0.18 Ga Karoo event and break up of Gondwana (Wilson et al., 1987). The 2575 Ma NNE- trending Great Dyke in the centre of the craton is one of the world's largest layered dyke-like intrusions, flanked by sub-parallel satellite dyke intrusions. These cross-cut mid-Archaean gneisses, late Archaean greenstone belts and late Archaean granitoid rocks. The Great Dyke is about 500 km long and up to 11 km wide, and the composition of the intruding magma is obscured by subsequent accumulation processes. The two main satellite dykes, referred to as the Umvimeela and the East satellite dykes, are mostly quartz gabbros. The southernmost discontinuous extension of the Great Dyke is called the Main satellite and comprises less accumulative feldspatic olivine websterites and melanorites. All three dykes extend 85 km into the northern marginal zone of the Limpopo belt. U-Pb dating of zircon and rutile from the Great Dyke gives an age of 2575.4 ± 0.7 Ma (Oberthür et al., 2002), identical with a recent baddeleyite U-Pb age of 2575.0 ± 1.5 Ma of the Umviveela dyke (Söderlund et al., in press)..

Another group of dykes in Zimbabwe are the NNW- trending Sebanga dykes which extend over larger parts of the craton. This swarm is approximately 500 km wide and 350 km long, made up of mostly vertical or near vertical dykes (Wilson et al., 1987). The largest dyke, the Sebanga Poort Dyke, is discontinuously 300 km long and about 80 m wide. It has been assumed that these dykes are feeder dykes to the ca. 1.9 Ga Mashonaland dolerite sheets. However, recent dating of dykes of the Sebanga swarm yield ages of 2408.3 ± 2.0 Ma, 2512.3 ± 1.8 Ma and 2470.0 ± 1.2 Ma (Söderlund et al., in press) demonstrating either a prolonged period of dyke intrusion or this swarm to host different generations of dykes.

The Mashonaland dolerites intrude the Archaean granite-greenstone basement as well as cross-cut the Great Dyke and its satellites in the northeastern part of the Zimbabwe craton. Geochemically, these dolerites are very different from the Great Dyke and its satellites (Stubbs et al., 1999). It is one of the most extensive Proterozoic sill complexes worldwide. Recent dating of these sills gave ages of 1885.9 ± 2.4 Ma, 1875.6 ± 1.8 Ma and 1878.1 ± 2.2 Ma (Söderlund et al., in press). Dykes that are possible age equivalent to the Mashonaland sill complex are the Mazowe dykes, which trend ESE across the northern part of the craton. This swarm is about 60-70 km long and 200 km long. The main dyke, called Mazowe River Dyke, is up to 60 m wide and about 120 km long. Geochemically, the Mazowe dykes appear to have been derived from a more depleted mantle source compared to the Mashonaland sills (Stubbs, 2000).

The Plumtree dyke swarm is roughly NNE-trending and approximately 450 km long and 70 km wide and comprise mostly ophitic dolerites. It is exposed across the western part of the craton, but is partly covered by younger sediments. It strikes north-south at its northern part but shifts gradually to a more northeasterly strike at its southern part. The emplacement age of the Plumtree dyke swarms is not known but could be feeders to ~2150 Ma Deweras Group basaltic lavas (Wilson et al., 1987).

2.3. Limpopo Belt

The Limpopo Belt is a 250 km wide ENE- trending collisional belt of granulite facies tectonites located in South Africa and Zimbabwe (Fig. 1). This belt separates the granitoid-greenstone terrains of the Kaapvaal craton and the Zimbabwe craton. The belt consists of a northern marginal zone, a Central Zone and a southern marginal zone. The southern marginal zone shows high-grade metamorphism and magmatic intrusions in the late Archaean between 2.69 Ga and 2.62 Ga (Kreissig et al., 2001) and is composed of tonalitic, trondjemitic and granodioritic plutons and minor greenstones, which were thrust onto the Kaapvaal craton along the Hout River shear zone (Zeh et al., 2007). In the northern marginal

zone, metamorphism and intrusion of plutons occurred between 2.72 Ga and 2.58 Ga (Berger et al., 1995). Orthogneisses with some greenstones and granitoid rocks were thrust onto the Zimbabwe craton along the Umlali shear zones (Zeh et al., 2007). The Central Zone, which is separated by major shear zones from the adjacent marginal zones, is dominated by granitoid gneisses and supracrustal rocks (3.3-2.5 Ga). The Palala shear zone bounds the Central Zone in the south whereas the Triangle shear zone bounds the Central Zone in the north. Both were formed under high-grade metamorphic conditions (granulite facies) at 2.0 Ga (Holzer et al., 1998) and underwent ductile deformation, followed by younger brittle reactivation. The Central Zone also shows high-grade metamorphism, anatexis, plutonism and ductile deformation. Metamorphism peaked within the Central Zone at ca. 2.0 Ga, and was followed by fast cooling and uplift (Jaeckel et al., 1997).

3. Analytical protocol

3.1. Geochronology

About 1 kg of dolerite sample was crushed with a sledge hammer and then milled in a swing mill to near -powder state. The sample was suspended in water. The smallest and heaviest grains, including the baddeleyite grains, with a range from 50 to 200, were separated from the rest of the sample using the Wilfley water-shaking table following the technique of Söderlund and Johansson (2002). The heavy mineral which concentrated was transferred into a Petri dish and the magnetic minerals including Fe-Mg minerals were removed with a strong pencil magnet wrapped in plastic. The baddeleyite grains were handpicked with forceps under a binocular microscope and then transferred using a small handmade pipette to another empty Petri dish, carefully sealed for secure transport to the Laboratory of Isotope Geology (LIG) in Stockholm.

The best-quality baddeleyite grains were transformed from the Petri to Teflon dissolution bombs using a handmade micropipette. The grains were carefully washed in warm ca. 3 N HNO_3 and then repeatedly in H_2O. A spike is a solution of unnatural isotopic composition of well-known concentrations and isotopic ratios. In the Stockholm laboratory, a spike of ^{205}Pb and $^{233\text{-}236}U$ was used. 1-2 drops of the spike and 10 drops of HF: HNO_3 (10:1) were added to the Teflon dissolution bombs. The dissolution bombs were covered and put into steel jackets, then put in the oven at 205°C for one day.

The samples were evaporated on a hot plate at ca. 100°C and dried down. Small 50 µl U-Pb columns were arranged in a column tray. In the beginning, water was added repeatedly to ensure that air was expelled from the columns. The ion exchange resin was then added to the U-Pb columns and washed extensively in steps using H_2O and 6,2 N HCl. Thereafter, the resin was conditioned using 3,1 N HCl. 10 drops of 3,1 N HCl were added to the samples in the Teflon dissolution bombs and dissolved before being loaded into the U-Pb columns. The Zr-Hf cut was washed out and collected in Savillex beakers for Hf isotope analysis (cf. Söderlund et al., 2006). Thereafter, U and Pb were collected into the Teflon dissolution capsules by adding a total of ca. 60 drops of H_2O in a number of steps. Eventually a small portion of H_3PO_4 was added before the sample was dried down on a hot plate at ca. 100°C.

The sample was then put on an outgassed Re filament. An automatic pipette adjusted to 2 µl was used. The pipette tip was first washed by rinsing in 2% HNO_3 4-5 times. The filament was put in the holder and the current was set to 1 A. The sample was dissolved in 2 µl of silica gel and then put on the filament using the cleaned pipette tip. The current was increased slowly until white smoke (the burned off H_3PO_4) rose up and a white salt was formed. The loading procedure was finished by increasing the current until it glowed shortly. The filament was then assembled in a sample holder wheel that fits into the mass spectrometer.

At the Museum of Natural History in Stockholm the samples were analysed in a Finnigan Triton thermal ionization multicollector mass spectrometer that can switch between Faraday cups and a Secondary Electron Multiplier (SEM), the latter of which is used to measure ^{204}Pb in static mode or in peak-switching mode for small samples. At ca. 1200°C a stable Pb signal was obtained and masses separated as the ion beam accelerated through a magnetic field. By adjusting the strength of the magnetic field, one could control what isotope was detected. The ion beam went through an analyser and was collected in the Faraday cups or the SEM. After measuring the Pb, the filament temperature was increased slowly to ca. 1350°C and U was measured in peak-switching mode. The mass spectrometer gave ratios of $^{206}Pb/^{204}Pb$, $^{206}Pb/^{207}Pb$, $^{206}Pb/^{205}Pb$ and $^{233}U/^{238}U$.

For plotting and age calculations, Ludwig's (2003) Isoplot version 3.0 was used. The correction of the initial common Pb was done according to Stacey and Kramers (1975). At a constant 0.1% per atomic mass unit, the mass discrimination was corrected for the Faraday and SEM detector.

To avoid contamination between samples, the Teflon dissolution bombs must be carefully washed in steps using strong acids. The first step was to add 30 drops of 6 N HCl into the capsules and put them covered in steel jackets for 2 days at 205°C. They were then emptied and 15 drops of HF and 15 drops of 7 N HNO_3 were added and again covered in steel in the oven at 205°C for 2 days. The next two steps were similar but used different acids. For the 3rd step, 20 drops of HF and 10 drops of 7 N HNO_3 were added, and for the 4th step 25 drops of HF and 5 drops of 7 N HNO_3 were added. After the last step, the acid was removed and 15-20 drops of H_2O were added after cooling down to room temperature.

3.2. Geochemistry

All 30 samples can - with the possible exception of some plagioclase-phyric intrusions- be regarded as representing melt compositions. All samples were first crushed and milled at either the University of KwaZulu -Natal or Lund University. A minimum of 10 g of fine powder from each sample was sent for major and trace element analysis to Acme Analytical Laboratories Ltd. (Vancouver, Canada). At Acme, approximately 0.2 g of powder sample was first fused in Lithium metaborate/tetraborate and then diluted in nitric digestion. These solutions were analysed on an ICP

emission spectrometry (major and some trace elements) and an ICP mass spectrometry (REE and other refractory elements). Another 0.5 g of each powder sample was decoct in Aqua Regia and then analysed by ICP Mass Spectrometry (precious and base metals). Resulting geochemical data are shown in Appendix 1.

4. Results

4.1. Geochronology

Geochronology using U-Pb on baddeleyite (ZrO_2) was performed on five samples of the NE-trending dykes of the Black Hills swarm in the northeast of the Bushveld Igneous Complex. Their approximate location can be seen in Fig. 2, with sample coordinates given in Table 2. The results are shown in Concordia diagrams in Fig. 3; the U-Pb isotopic data is listed in Table 1; a summary of their ages, trends and sample locations is displayed in Table 2.

Common for all these samples are, first, a low abundance of baddeleyite and, second, a variable degree of secondary alteration often seen as a thin rim of secondary zircon. This means that most data is moderately to strongly discordant, presumably due to the transition of baddeleyite to rim zircon during alteration or low-degree metamorphism.

Additional analyses of most of these samples, as well as other dykes of the NE- to ENE-

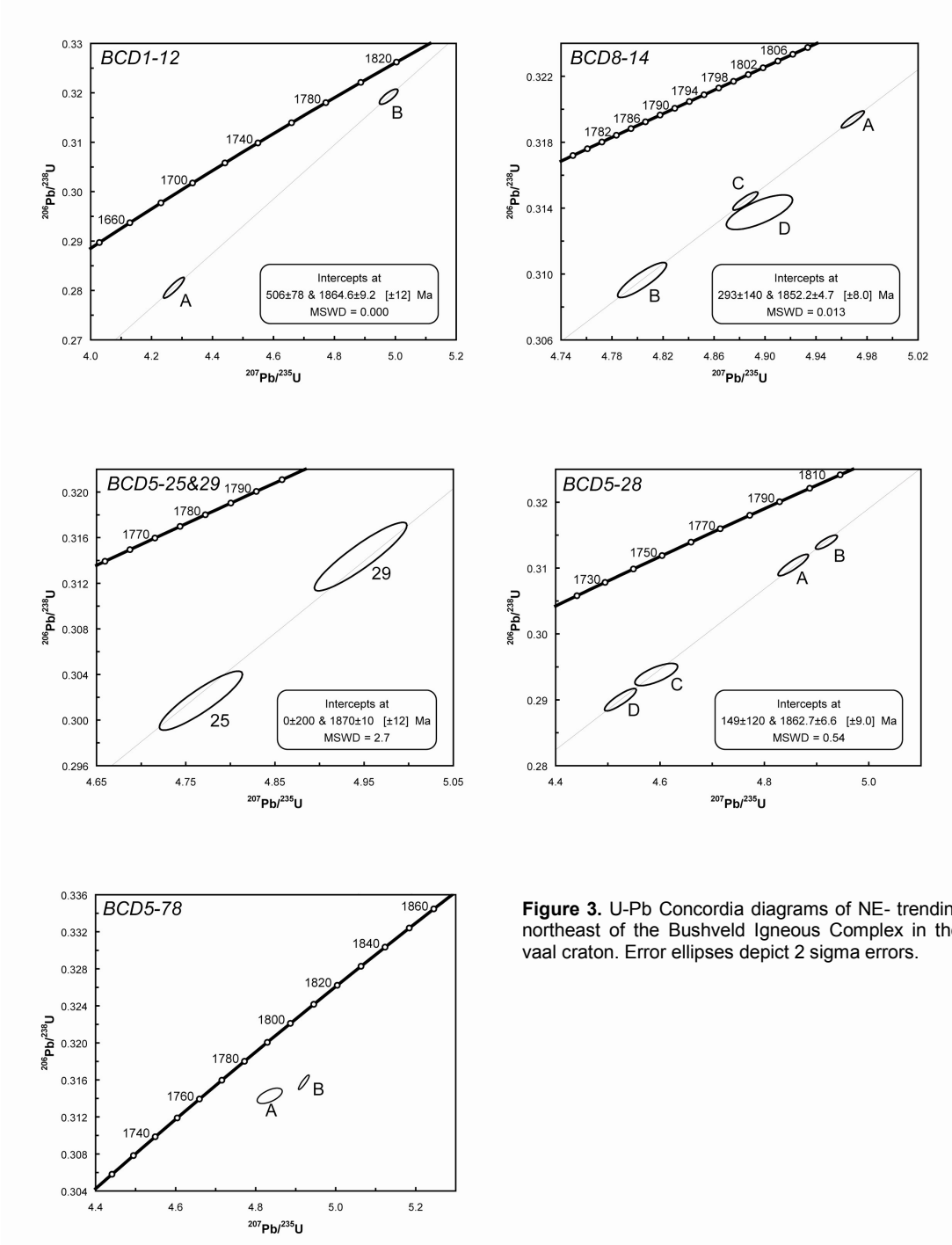

Figure 3. U-Pb Concordia diagrams of NE- trending dykes northeast of the Bushveld Igneous Complex in the Kaapvaal craton. Error ellipses depict 2 sigma errors.

Table 1. U-Pb isotopic table

Mineral type[1)]	U/Th	Pbc/Pbtot[2)]	$^{206}Pb/^{204}Pb$ raw[3)]	$^{207}Pb/^{235}U$ [corr][4)]	± 2s % err	$^{206}Pb/^{238}U$ [corr][4)]	± 2s % err	$^{207}Pb/^{235}U$ [age, Ma]	$^{206}Pb/^{238}U$ [age, Ma]	$^{207}Pb/^{206}Pb$ [age, Ma]	± 2s Ma	Concord-ance
BCD1-12												
Bd-a (11 k)	6.3	0.046	1390	4.2729	0.65	0.28055	0.61	1688.2	1594.1	1807.0	5.1	0.866
Bd-b (11 k)	8.0	0.129	418	4.9781	0.50	0.31922	0.38	1815.6	1785.9	1849.9	5.5	0.929
BCD5-25												
Bd (3k)	3.0	0.279	191	4.7670	0.80	0.30170	0.70	1779.1	1699.7	1873.5	6.5	0.834
BCD5-29												
Bd (6k)	3.1	0.246	227	4.9462	0.86	0.31434	0.78	1810.2	1762.0	1866.1	6.3	0.884
BCD5-28												
Bd-a (4k)	8.8	0.093	612	4.8552	0.49	0.31046	0.43	1794.5	1743.0	1855.0	4.1	0.914
Bd-b (6k)	5.5	0.076	714	4.9188	0.34	0.31393	0.28	1805.5	1760.0	1858.4	3.6	0.925
Bd-c (4k)	6.5	0.196	264	4.5928	0.73	0.29385	0.47	1748.0	1660.7	1853.9	9.3	0.842
Bd-d (5k)	5.9	0.158	340	4.5241	0.55	0.29002	0.48	1735.4	1641.6	1850.4	5.0	0.843
BCD5-78												
Bd-a (5)	7.3	0.172	303	4.8350	0.53	0.31432	0.22	1791.0	1761.9	1825.1	8.0	0.916
Bd-b (10)	12.2	0.034	1717	4.9204	0.23	0.31577	0.20	1805.8	1769.1	1848.4	1.7	0.945
BCD8-14												
Bd-a (5k)	17.7	0.017	3518	4.9688	0.15	0.31938	0.13	1814.0	1786.7	1845.6	1.2	0.961
Bd-b (4k)	9.2	0.062	927	4.8036	0.33	0.30964	0.28	1785.5	1738.9	1840.4	2.9	0.926
Bd-c (5k)	18.0	0.022	2783	4.8846	0.16	0.31444	0.14	1799.6	1762.5	1842.9	1.5	0.947
Bd-d (7k)	10.3	0.125	433	4.8957	0.43	0.31375	0.27	1801.5	1759.1	1850.9	5.5	0.914

[1)] Bd = baddeleyite, (x) = number of grains in each analysis.

[2)] Pbc = common Pb; Pbtot = total Pb (radiogenic + blank + initial).

[3)] measured ratio, corrected for fractionation and spike.

[4)] isotopic ratios corrected for fractionation (0.06% per amu for Pb), spike contribution, blank (2 pg Pb and <1 pg U), and initial common Pb. Initial common Pb corrected with isotopic compositions from the model of Stacey and Kramers (1975) at 1850 Ma.

Table 2. Summary of samples dated in this study.

Sample	Latitude	Longitude	Dyke trend	Age (Ma), error (2σ)
BCD5-25	23°46'40.55" S	30°39'29.63" E	20°	1870 ± 10[2)]
BCD5-29	23°39' 7.13" S	30°43'49.87" E	20°	1870 ± 10[2)]
BCD1-12	24°24'21.31" S	30°47'50.57" E	57°	1865 ± 9[2)]
BCD5-28	23°39'20.63" S	30°43'49.87" E	30°	1863 ± 7
BCD8-14[1)]	23°59'14.37" S	31° 7'32.38" E	uncertain	1852 ± 5
BCD5-78	24°12'25.27" S	30°50'10.64" E	35°	≥ ca. 1848[3)]

[1)] Sample collected at the Foskor PTY mine in Phalaborwa.

[2)] Intercept age comprising regression of 2 analyses. Age should be treated as approximate

[3)] The ca. 1848 Ma date is the $^{207}Pb/^{206}Pb$ age of the least discordant analysis.

trending dykes of the Black Hills swarm, were conducted by Johan Olsson during the fall of 2009 at the Jack Satterly Laboratory in Toronto, Canada.

4.1.1. BCD1-12

The low number of grains extracted from this sample allowed for only two fractions of 11 crystals each to be analysed. Regression yields an upper intercept of 1865 ± 9 Ma and a lower intercept of 506 ± 78 Ma (Fig. 3). Although only two fractions were analysed, the result demonstrate this dyke belongs to the 1.87-1.85 Ga suite of dykes in this part of Kaapvaal. The $^{207}Pb/^{206}Pb$ age of ~1846 Ma for the least discordant fraction is taken as a minimum age for crystallisation of this dolerite dyke.

4.1.2. BCD8-14

Regression of three fractions of 4 to 5 grains each yields an upper intercept age of 1852 ± 5 Ma and a lower intercept age of 293 ± 140 Ma (Fig. 3). The forth analysis (the D-fraction) with 7 grains plots slightly below the Discordia line and is not included in the regression. This analysis is associated with a large analytical error and has much higher amount of common Pb relative to radiogenic Pb than the other analyses.

4.1.3. BCD5-25 and BCD5-29

An upper intercept age of 1870 ± 10 Ma is derived from using a lower intercept forced through 0 ± 200 Ma (Fig. 3), which yields an acceptable MSWD value of 2.7. The two fractions of 3 and 6 grains each were separated from samples taken from different localities, but are from the same dyke like it can be seen in Fig. 4. The age estimate can only be taken as approximate since only two analyses are used in the regression.

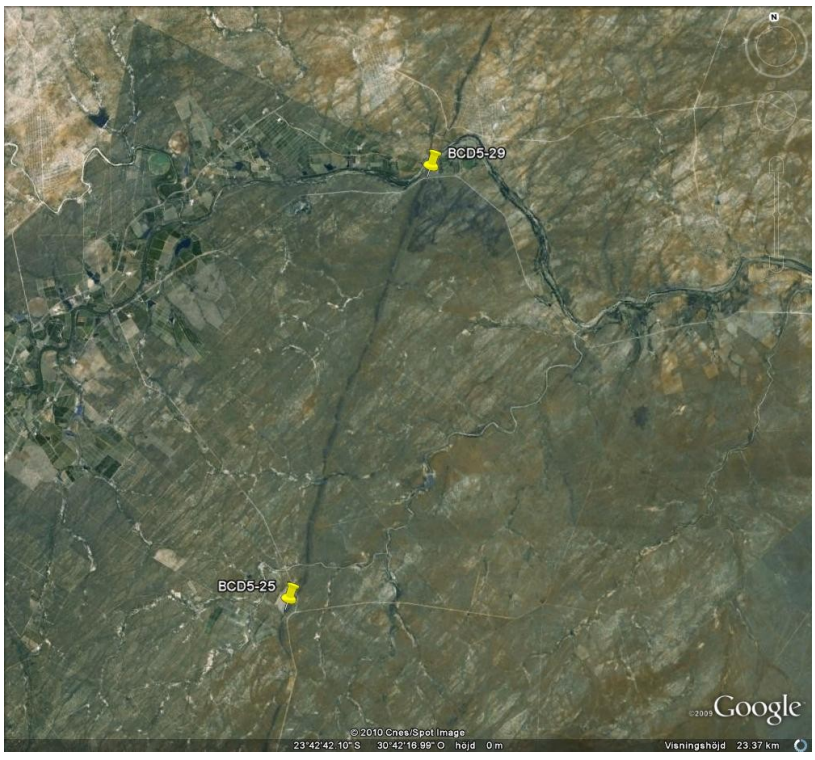

Figure 4. Google map showing samples BCD5-25 and BCD5-29 of the Black Hills swarm belong to the same dyke.

4.1.4. BCD5-28

Analyses of four fractions with 4-6 grains each gives an upper intercept age of 1863 ± 7 Ma (Fig. 3; MSWD = 0.54). This age is interpreted as the emplacement age of the dyke.

4.1.5. BCD5-78

These two analyses with 5 and 10 grains plot very close to each other and, combined with significant discordance, make regression meaningless (Fig. 3). Although no final age can be assigned the $^{207}Pb/^{206}Pb$ age of 1848.4 ± 1.7 Ma for the B-fraction is interpreted as the minimum age of this sample.

4.2. Geochemistry

30 samples were analysed according to the procedures specified in Section 3.2. These samples are mainly subdivided into four groups of: 2.7 Ga dykes that are geochemically more primitive (red triangles) and more evolved (green triangles), as well as ca. 1.87– 1.85 Ga dykes that are geochemically more primitive (violet diamonds) and more evolved (blue squares). Their location is shown on a sample location

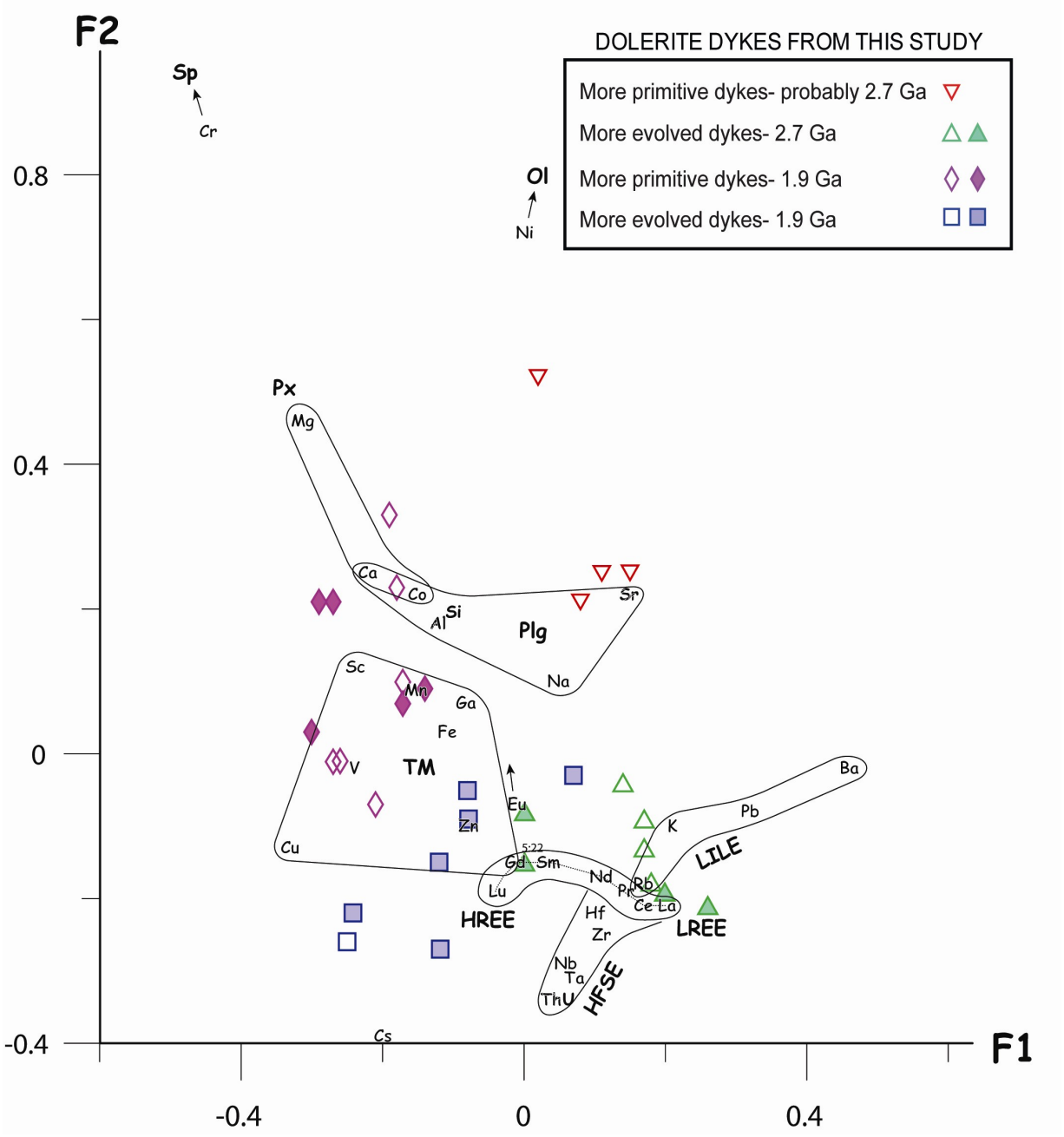

Figure 5. Correspondence analysis results for F1 and F2 of all variation between the 30 samples of this study. F1 and F2 (Factors 1 and 2) display ~43% and ~27% of the total inertia from a correspondence analysis on a data array of 10 major elements and 34 trace elements, performed by the ViSta © freeware by Forrest W. Young (http://forrest.psych.unc.edu/research/index.html). LREE= Light rare earth elements, HFSE= High field strength elements, LILE= Large– ion lithophile elements.

map (Appendix 2). Figure 5 shows the subdivision into these groups is based on known ages and how samples cluster around these after a correspondence analysis; i.e., samples that plot closer together have more similar compositions than those plotting farther apart. Correspondence analysis is both an exploratory and multivariate descriptive data analytical technique (Benzecri, 1992; Clausen, 1998; Davis, 2002; Greenacre 1984, 1993), which can be applied on any data array (i.e., rows and columns) such as in our

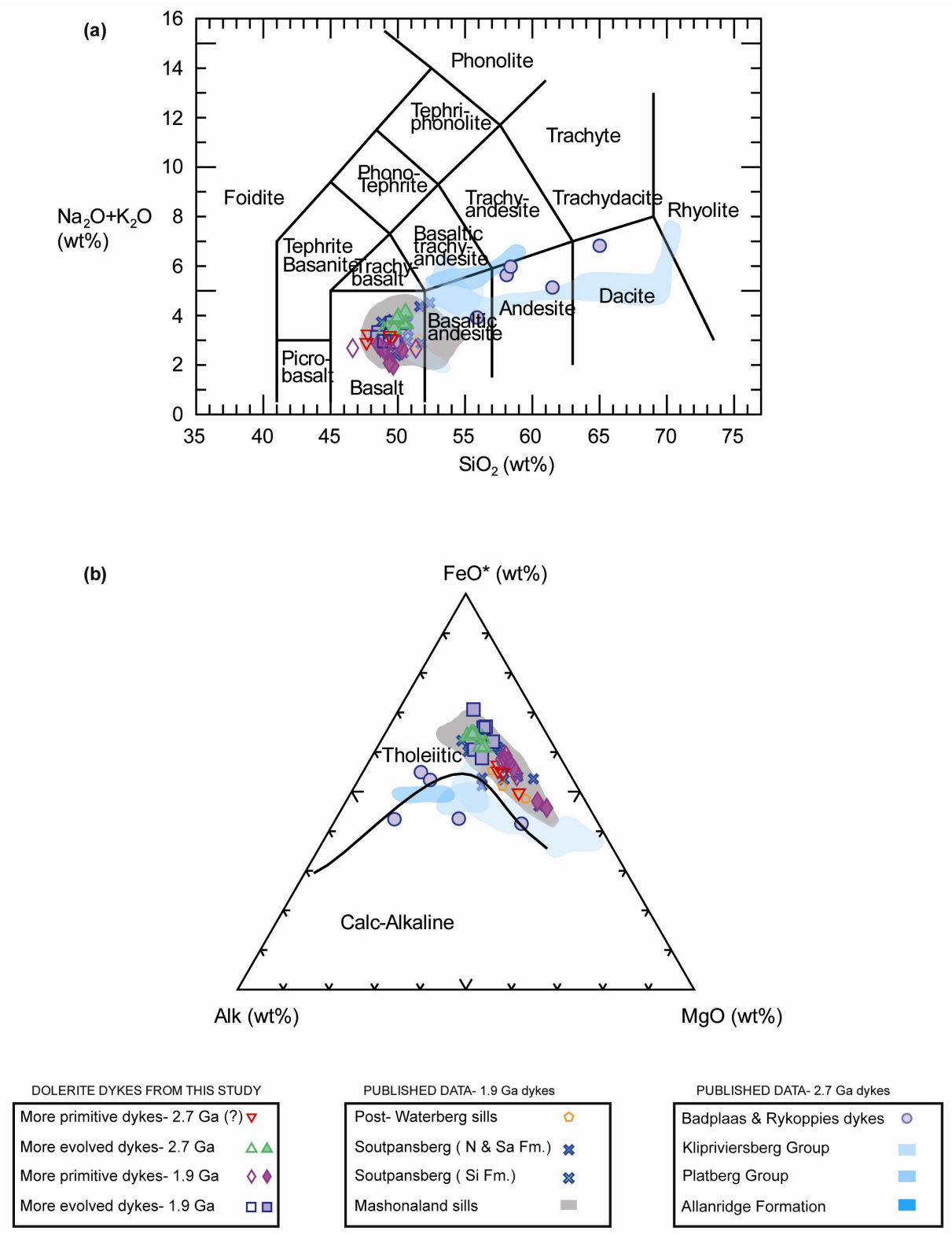

Figure 6. (a) TAS- diagram after LeBas et al. (1986), (b) AFM- diagram after Irvine and Baragar (1971). N & Sa Fm. and Si Fm. in the legend stand for Ngwanedzi & Sabasa Formation and Sibasa Formation, respectively.

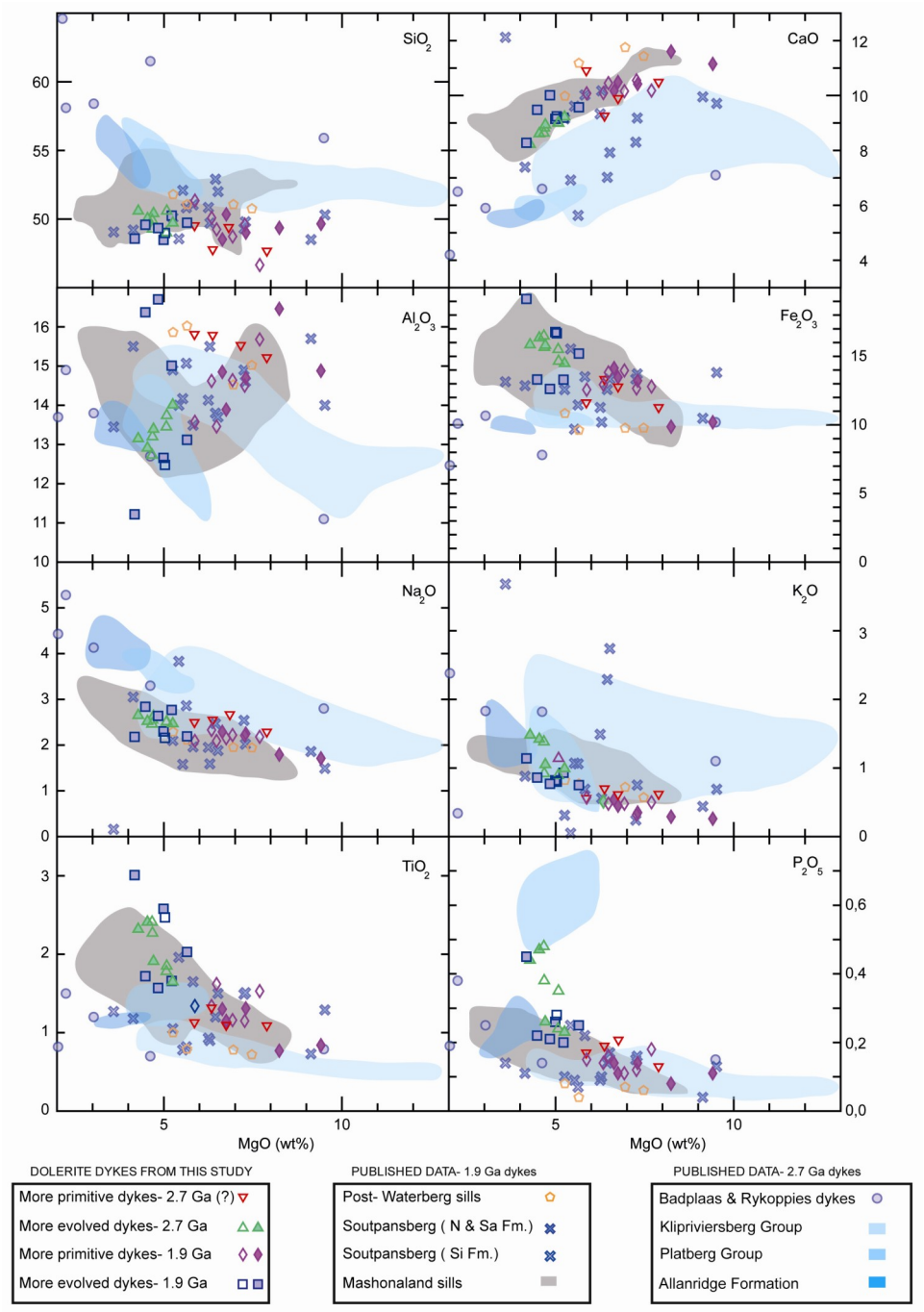

Figure 7. Variation diagrams plotting several major elements against MgO, which here is used as a differentiation index. All values in weight % (cf., Appendix 1). N & Sa Fm. and Si Fm. in the legend stand for Ngwanedzi & Sabasa Formation and Sibasa Formation, respectively.

suite of 10 major and 34 trace elements on 30 samples (Appendix 1). It may be viewed as a type of (Chi square) principal components analysis that aims at displaying variations within rows and columns within a contingency table graphically. Thus, statistical variances (also expressed as eigenvalues) are expressed as relative distances along axes that determine these dimensions of factors. The greatest variances (expressed as the highest percentage of the total inertia) is displayed along the first, so called, Factor (or Dimension) axis (F1 in Fig. 5), whereas corresponding less variance is expressed along successively higher dimensions. Commonly, most important variations within a petrogenetically related geochemical data set is displayed by the first two to three Factor axes. This is also the case in Fig. 5, where we can see that there is (1) a major variance between more or less evolved dyke samples, controlled by more or less compatible and incompatible elements, and (2) a lesser variance between samples that appear to be more (2.7 Ga dykes) or less (1.87– 1.85 Ga dykes) LILE-enriched (cf., Klausen et al, in press). The results of this analysis are shown in Appendix 3. Samples that have been dated in this study (only 1.87– 1.85 Ga dykes), by Olsson et al. (in press, unpublished data) and Söderlund et al. (in press), are high-lighted as filled symbols.

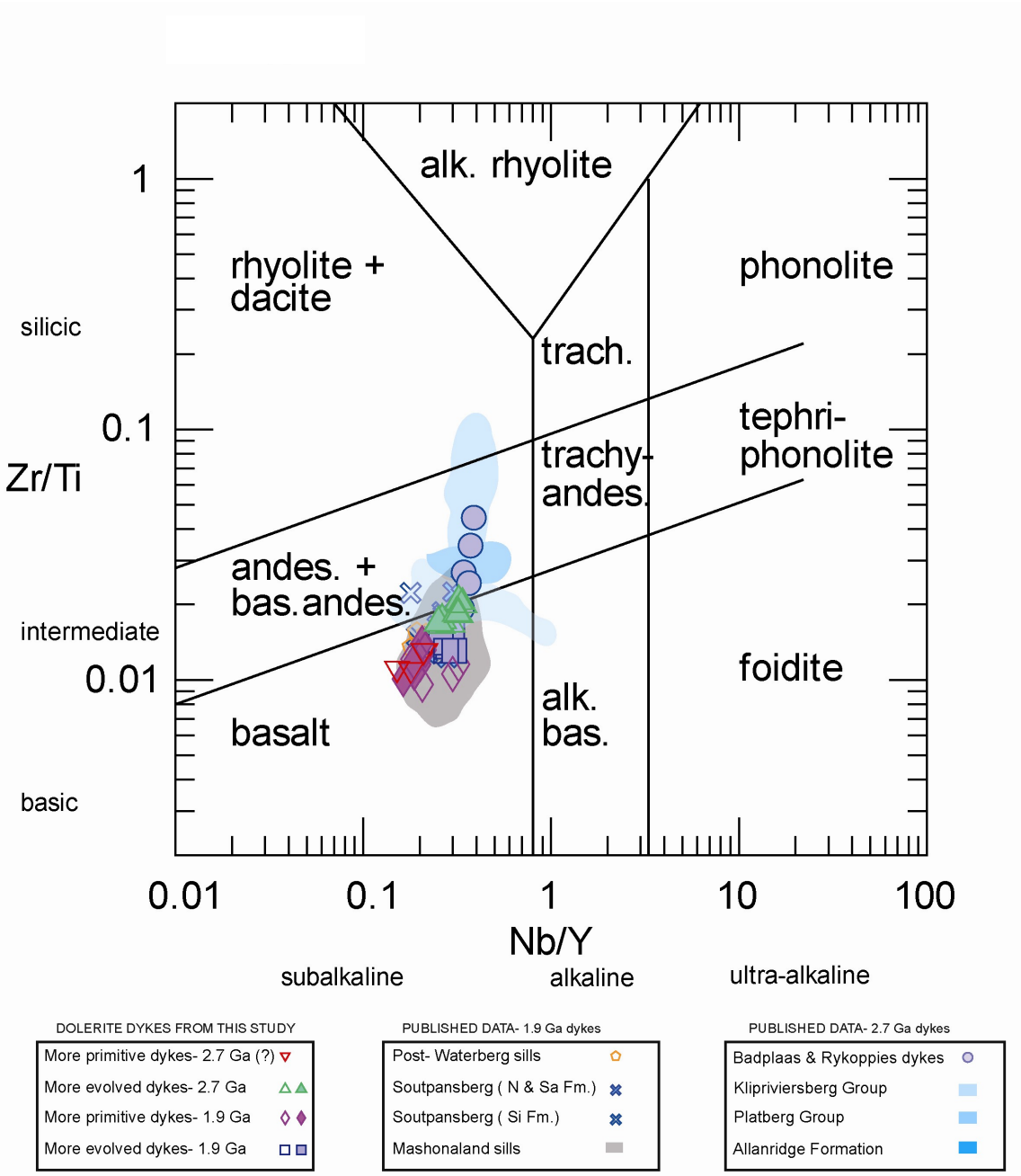

Figure 8. Nb/Y vs. Zr/Ti diagram after Pearce (1996). N & Sa Fm. and Si Fm. in the legend stand for Ngwanedzi & Sabasa Formation and Sibasa Formation, respectively.

Published data on post- Waterberg sills (Hanson et al., 2004b), Soutpansberg lavas (Bumby et al., 2001; Crow and Condie, 1990) and Mashonaland sills (Stubbs et al., 1999; XRF) are added for comparisons with the largely coeval 1.9 Ga dykes. The 2.7 Ga dykes are compared to coeval dykes from the Rykoppies area and Badplaas-Barberton area (Klausen et al., in press) and Ventersdorp lavas (Crow and Condie, 1988; Marsh et al., 1992; Nelson et al., 1992).

4.2.1. Major elements

A TAS diagram [Fig. 6 (a)]; LeBas et al., 1986) determines that all dyke rock samples are sub-alkaline basalts. Some of the Soutpansberg lavas, Mashonaland and post- Waterberg sill samples plot across the border into the basaltic andesite field. The AFM diagram (Fig. 6 (b); Irvine and Baragar, 1971), furthermore, shows that almost all of the samples belong to an Fe-enriched tholeiitic trend, with only two basaltic andesite Soutpansberg lava sample plotting on the border to the calc alkaline field. Thus, it can be concluded that both 2.7 Ga and ca. 1.87– 1.85 Ga dykes, as well as coeval lavas and sills, are predominantly tholeiitic basalts, evolving towards becoming basaltic andesites.

The 2.7 Ga dykes from this study differ significantly from other roughly coeval dykes from the Rykoppies area and Badplaas-Barberton area and Ventersdorp lavas, which are more calc-alkaline ba-

saltic andesites to dacites (Fig. 6; Klausen et al., in press). In this aspect the rock type classification diagrams cannot discriminate between ca. 1.87– 1.85 Ga and 2.7 Ga dykes from this study.

MgO is chosen as a differentiation index (Fig. 7) because this major element decreases the most (ranging from 2.6 till 9.4 wt%) during fractionation of Mg-rich minerals (e.g., olivine and/or pyroxene) within such basaltic magmas. Again, there are no significant differences between ca. 1.87– 1.85 Ga and 2.7 Ga dykes, just that the more evolved samples from each age group have lower MgO contents. The SiO_2 content remains nearly constant during differentiation, ranging between 47-50 wt%. Some of the more andesitic Mashonaland sills show slightly higher SiO_2 content up to 55 wt% and Ventersdorp samples show even higher SiO_2 contents up till 71 wt%. The alkalies increase with decreasing MgO, from 1.7 to 2.8 wt% for Na_2O and 0.3 to 1 wt% for K_2O, the latter of which reflecting a more than two-fold incompatible element enrichment during differentiation. Some Soutpansberg lava samples have anomalously high K_2O compared to the trend defined by the rest of the data, which probably is due to secondary addition of the more mobile K_2O. The Ventersdorp lavas and Badplaas and Rykoppies dykes have generally higher contents of alkalies than most of the other data. CaO decreases from 11.6 to 8.2 wt% with decreasing MgO, consistent with some fractionation of Ca-rich minerals (e.g., clinopyroxene and/or plagioclase). The Soutpansberg dolerites have mostly lower CaO contents at similar MgO, whereas the post- Waterberg sills have slightly

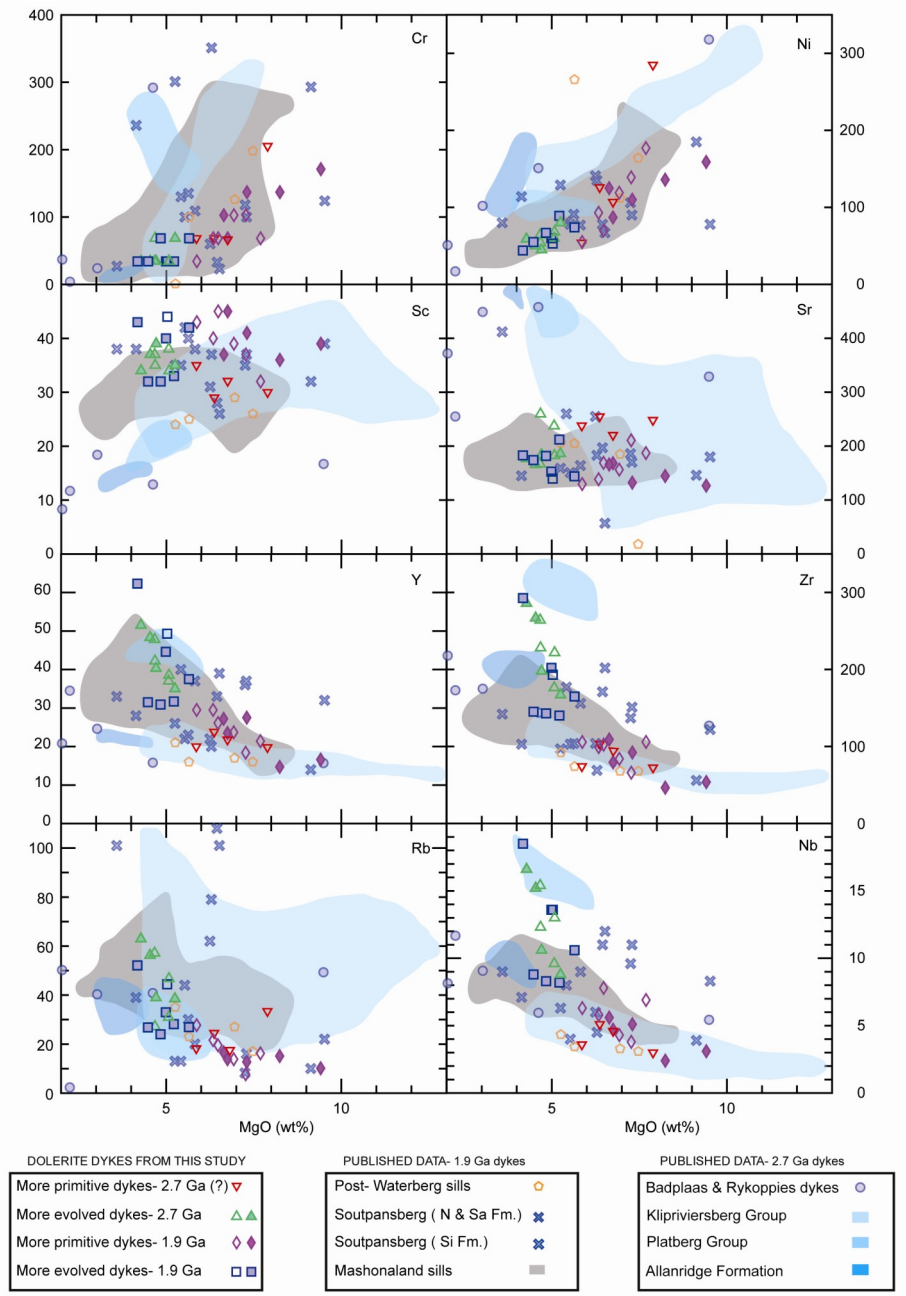

Figure 9. Variation diagrams plotting several trace elements against MgO, used as a differentiation index. All values in ppm (cf., Table 3). Some samples from ca. 2.7 Ga published data were left out in the Cr and Ni diagram due to too high values. N & Sa Fm. and Si Fm. in the legend stand for Ngwanedzi & Sabasa Formation and Sibasa Formation, respectively.

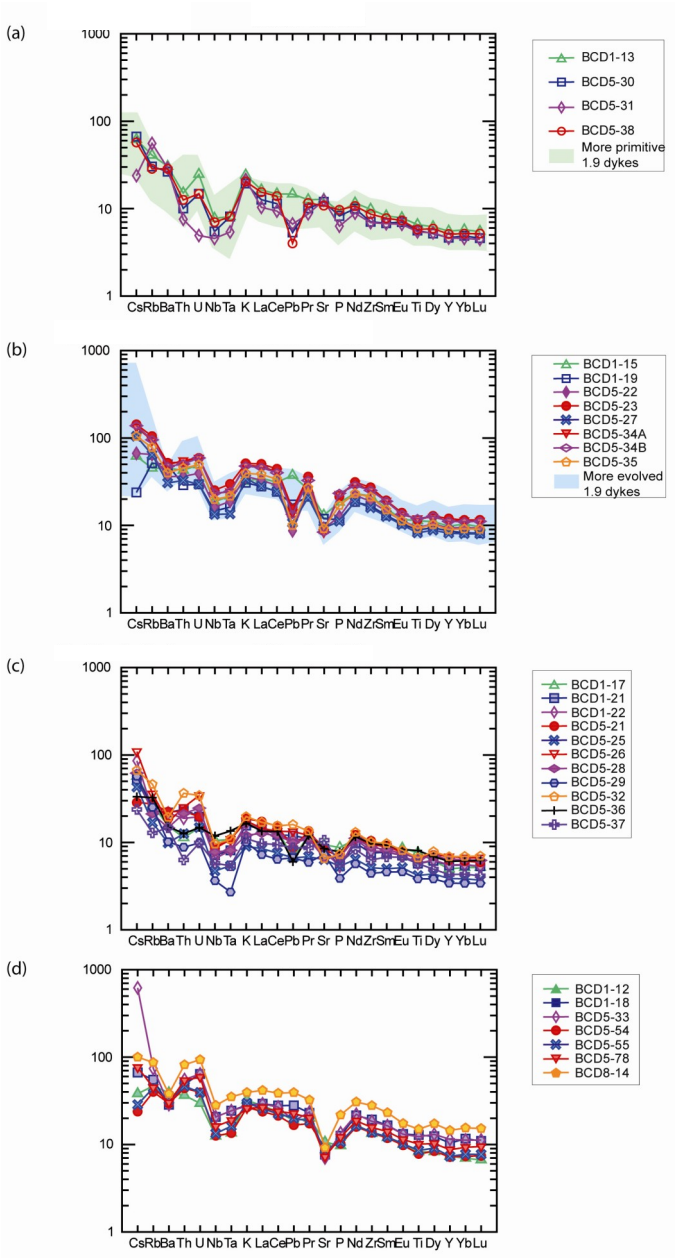

Figure 10. Primitive mantle normalised multi elements diagrams from this study after MacDonough and Sun (1995) for: (a) more primitive 2.7 Ga dykes with a shaded background representing the 1.9 Ga samples; (b) more evolved 2.7 Ga dykes with a shaded background representing the 1.9 Ga samples; (c) more primitive 1.9 Ga dykes; (d) more evolved 1.9 Ga dykes.

higher CaO contents. The 2.7 Ga dykes of the published data have lower CaO contents than samples from this study. The less evolved ca. 1.87– 1.85 Ga and 2.7 Ga dykes also shows a decreasing Al_2O_3 (between 11.2 and 16.7 wt%) with decreasing MgO, indicating relatively early fractionation of plagioclase (±clinopyroxene and/or some other Mg-rich phase). Some of the more evolved 2.7 Ga and ca. 1.87– 1.85 Ga samples deviate from this plagioclase fractionation trend by exhibiting more elevated Al_2O_3; tentatively attributed to the possible accumulation of plagioclase. Likewise, the Mashonaland sills also exhibit an early Al_2O_3 decrease with increasing MgO, followed by an unexpected Al_2O_3 increase that may, likewise, be attributed to some plagioclase accumulation in more evolved intrusions. This interpretation is substantiated by these intrusions commonly being plagioclase-phyric. Ventersdorp lavas show in contrast increasing Al_2O_3 trends with decreasing MgO.

The Fe_2O_3 content (10.4-20.1 wt%) is slightly increasing with decreasing MgO, consistent with the tholeiitic trend in Fig. 6 (b) that normally is caused by more delayed magnetite fractionation, compared to calc-alkaline magma series. This is also consistent with increasing TiO_2 (0.8-3.0 wt%) with decreasing MgO, reflecting delayed ilmenite fractionation. Likewise, increasing P_2O_5 (0.1-0.5 wt%,) with decreasing MgO is consistent with the lack of any apatite fractionation. Compared to less evolved samples, more evolved ca. 1.87– 1.85 Ga and 2.7 Ga samples exhibit slightly steeper trends towards higher P_2O_5 and TiO_2 values. Thus, some of the Soutpansberg lava samples and most of the post-Waterberg/Mashonaland sills show lower P_2O_5 values than the dyke samples of this study, at similar MgO.

In general the major element trends are consistent with the fractionation of some unspecified Mg-rich phase (olivine and/or pyroxene) as well as plagioclase fractionation (decreasing CaO and Al_2O_3) and local accumulation.

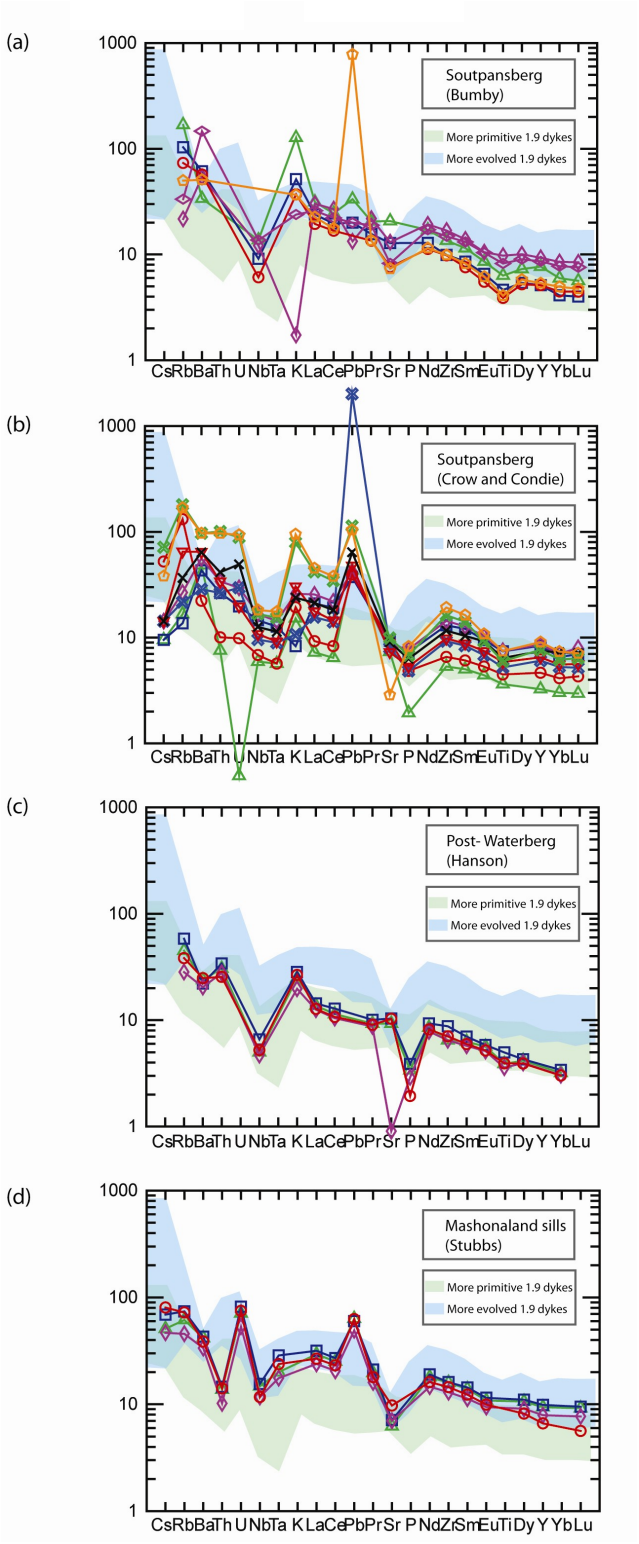

Figure 11. Primitive mantle normalised multi elements diagrams after MacDonough and Sun, 1995 with shaded background representing the samples of this study for: (a) Soutpansberg lava samples (Bumby et al., 2001); (b) Soutpansberg lava samples (Crow and Condie, 1990) post-Waterberg samples (Hanson et al., 2004b);
(d) Mashonaland sill samples (Stubbs et al., 1999).

4.2.2. Trace elements

Another way to classify the samples with the help of trace elements is to use the Nb/Y vs. Zr/Ti diagram after Pearce, 1996 (Fig. 8). The Nb/Y vs. Zr/Ti diagram has an advantage over the TAS- diagram in its usage of more immobile elements. Fig. 8 shows that most of the samples still classify as sub-alkaline basalts like in the TAS-diagram indicating that our samples have not suffered secondary LILE mobilisation. Some of the Soutpansberg samples and some of the Mashonaland sill samples (grey area) plot in the andesite + basaltic andesite field. The more evolved 2.7 Ga samples are on the border to the andesite + basaltic andesite field, whereas other coeval dykes clearly plot in the andesite + basaltic andesite field (Klausen et al., in press). In comparison to the TAS-diagram (Fig. 6 (a); LeBas et al., 1986), the samples in Fig. 8 plot closer to the border of the andesite + basaltic andesite field.

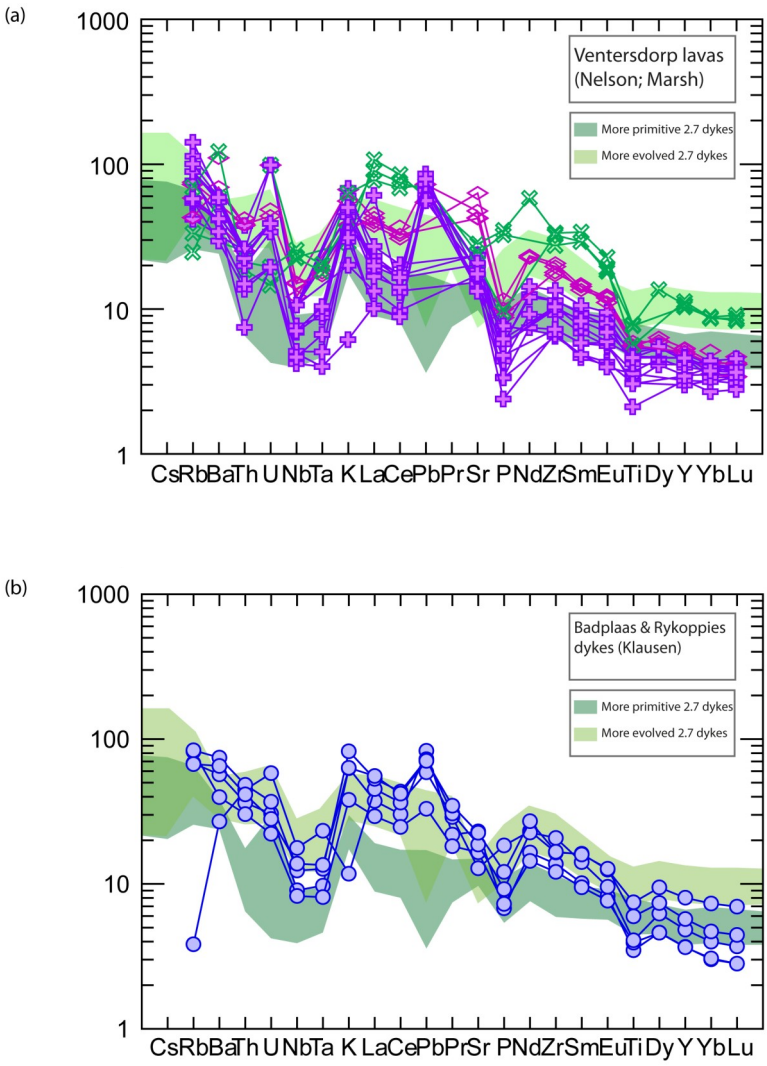

Figure 12. Primitive mantle normalised multi elements diagrams after MacDonough and Sun, 1995 with shaded background representing the 2.7 Ga samples of this study for: (a) Ventersdorp lavas (Nelson et al., 1992; Marsh et al., 1992); (b) Rykoppies and Badplaas-Barberton dykes (Klausen et al., in press).

As for the major elements, selected trace elements are plotted against MgO as a differentiation index (Fig. 9). Cr was measured as Cr_2O_3 (wt%) but is converted to Cr (ppm), using the following formula:

$Cr = Cr_2O_3 \times (52/152) \times 10000$

Cr (34-274 ppm) is mostly decreasing with decreasing MgO but also show horizontal trends that reflect poor analytical accuracy close to the analytical detection limit. The general decreasing trend, however, is still consistent with the fractionation of pyroxene and/or Cr -spinel. Some of the Soutpansberg samples show higher Cr concentrations, possibly due to the accumulation of these phases. The Klipriviersberg samples have the highest Cr contents which seems to be a real liquid trend. The Ni content (22-285 ppm) also decreases with decreasing MgO, consistent with olivine and/or pyroxene fractionation. The Sc concentration (29-45 ppm) and the Sr concentration (130-260 ppm) do not show any clear depletion trend, as would be expected from pyroxene and plagioclase fractionation, respectively. The ca. 1.87– 1.85 Ga samples show mostly slightly higher Sc and lower Sr concentrations than the 2.7 Ga samples, which could indicate that the ca. 1.87– 1.85 Ga samples have experienced more clinopyroxene and less plagioclase fractionation, respectively, or that there are differences between LILE

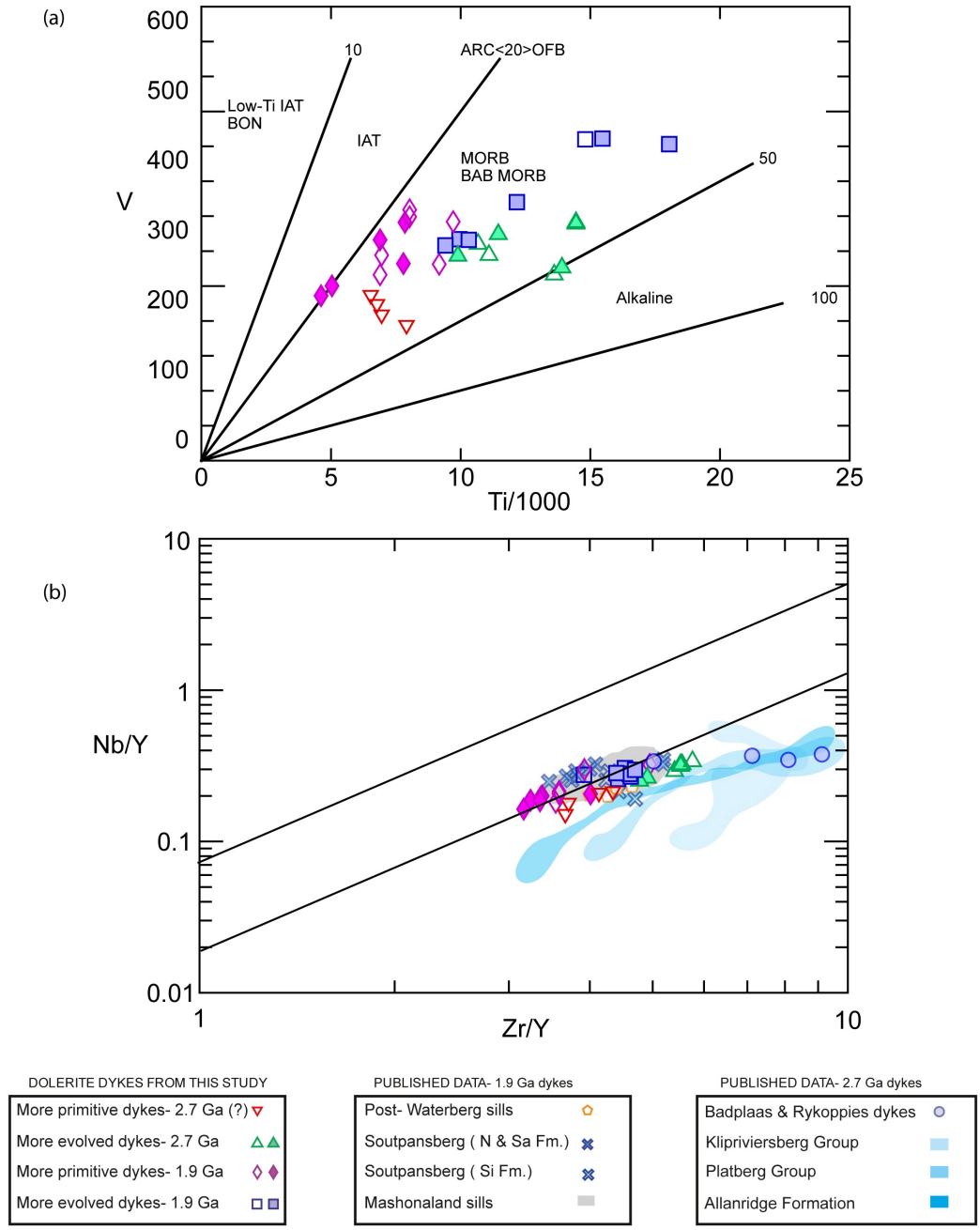

Figure 13. (a) Ti vs. V diagram after Shervais (1982), (b) Nb/Y vs. Zr/V diagram; the parallel lines show the limits of the Iceland data from Fitton et al. (1997). N & Sa Fm. and Si Fm. in the legend stand for Ngwanedzi & Sabasa Formation and Sibasa Formation, respectively.

and transitional elements in the source composition. The commonly incompatible Y, Zr, Rb and Nb all increase with decreasing MgO, by as much as a five-fold increase in Zr and Nb between the most primitive and most evolved samples. The dykes may have slightly lower Rb (LILE) values and slightly higher Y, Zr and Nb (HFSE), compared to the published data on lavas and sills.

Four primitive mantle normalised multi-element diagrams (MacDonough and Sun, 1995) show the chemical differences between the four main groups; i.e., less and more evolved ca. 1.87– 1.85 Ga and 2.7 Ga samples. All samples (Fig. 10) generally exhibit parallel patterns within each of the 4 groups but also between all of the samples of every group with few exceptions, which will be emphasised later. All samples are both LILE enriched and show negative Nb-Ta anomalies. LILE- enriched patterns with distinctly negative Nb-Ta anomalies are typically produced in subduction zone settings, but this is difficult to reconcile with the more tholeiitic major element compositions and intra-cratonic setting of both 2.7 Ga and ca. 1.87– 1.85 Ga intrusions. Thus, it is suspected that these patterns reflect the involvement of the continental lithosphere, either through crustal assimilation and/or the partial melting of a metasomatised sub-continental lithospheric mantle (SCLM). The more evolved ca. 1.87– 1.85 Ga samples (Fig. 10 (d)) do

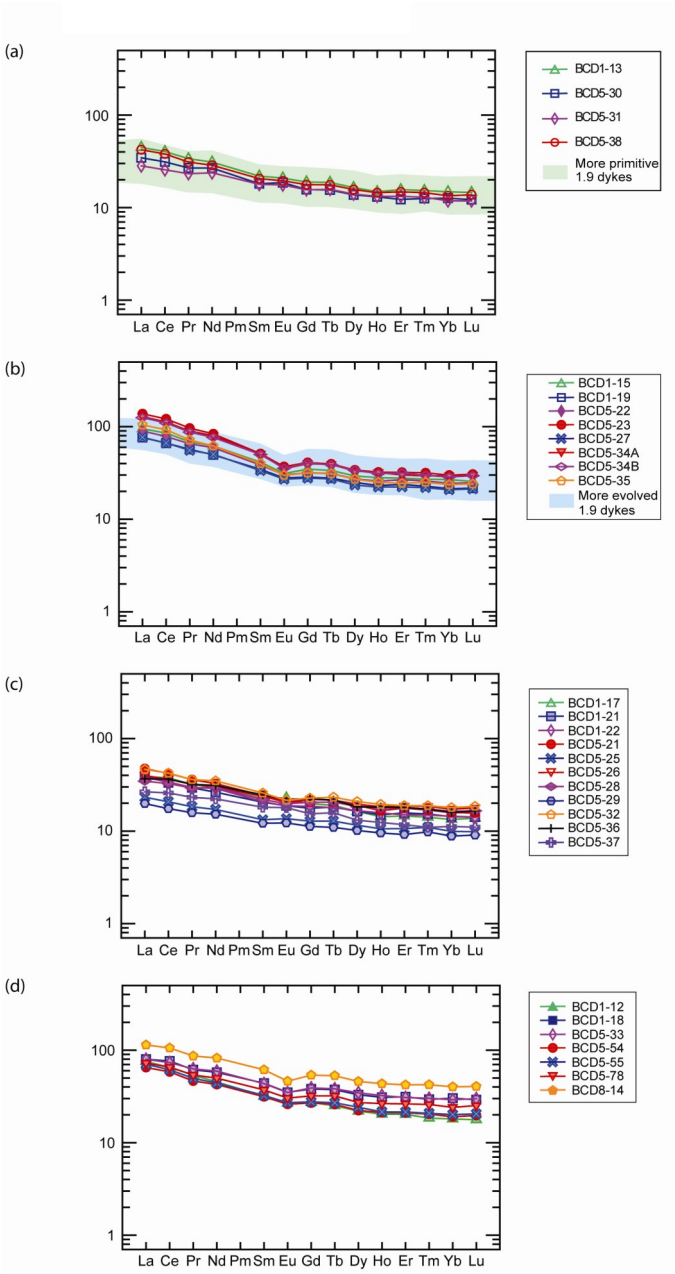

Figure 14. Chondrite normalised REE diagrams from this study after Sun and MacDonough(1989) for: (a) more primitive 2.7 Ga dykes with a shaded background representing the 1.9 Ga samples; (b) more evolved 2.7 Ga dykes with a shaded background representing the 1.9 Ga samples; (c) more primitive 1.9 Ga dykes; (d) more evolved 1.9 Ga dykes.

not have such distinctive Nb-Ta anomalies as the other groups and have a flatter LILE profile, suggesting perhaps a lower proportion of continental lithosphere. Furthermore, all samples also have a negative P-anomaly which is indicative of apatite fractionation, contrary to what was inferred from Fig. 7. The 2.7 Ga samples show a negative Pb-anomaly whereas the ca. 1.87– 1.85 Ga samples show mostly none. A negative Sr anomaly is shown for the more evolved 2.7 Ga (Fig. 10 (b)) and ca. 1.87– 1.85 Ga (Fig. 10 (d)) which is consistent with the plagioclase fractionation inferred from Fig. 7.

The primitive mantle normalised multi-elements diagram for the Soutpansberg lava samples (Fig. 11 (a)-(b); Bumby et al., 2002; Crow and Condie, 1990), the post-Waterberg samples (Fig. 11 (c); Hanson et al., 2004b) and the Mashonaland sill samples (Fig. 11 (d); Stubbs et al., 1999) are also all generally LILE-enriched. The samples from Crow and Condie (1990) and the Mashonaland sills show positive Pb anomalies, unlike the samples of this study. Additionally they also both show negative Nb-Ta anomalies. Bumby et al.'s (2002) and Hanson et al.'s (2004b) samples also show negative Nb anomalies (Ta was not measured in these samples). The Soutpansberg lava samples from Crow and Condie (1990) and the post-Waterberg samples from Hanson et al. (2004b) have slightly negative Ti and P anomalies. Negative Sr anomalies can be seen in all the Soutpansberg lava samples (Fig. 11 (a)-(b); Bumby et al., 2002; Crow and Condie, 1990) and the Mashonaland sills. Most of the described features of the published data can also be seen in samples of this study.

Primitive mantle normalised multi-elements diagram of Ventersdorp lavas (Fig. 12 (a); Nelson et al., 1992; Marsh et al., 1992) and roughly coeval dykes from the Rykoppies and Badplaas- Barberton area (Fig. 12 (b); Klausen et al., in press) are also generally LILE- enriched and show negative Nb-Ta, P- and Ti-anomalies. The samples from Crow and Con-

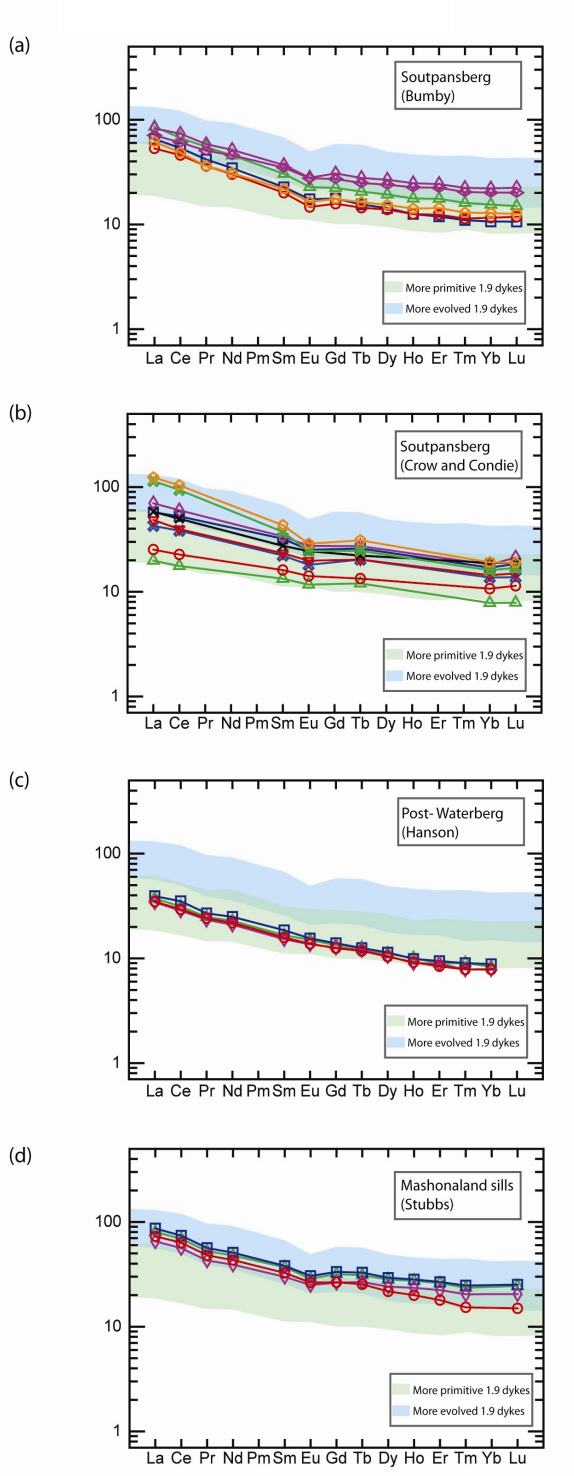

Figure 15. Chondrite normalised REE diagrams after Sun and MacDonough (1989) with shaded background representing the samples of this study for: (a) Soutpansberg lava samples (Bumby et al., 2002); (b) Soutpansberg lava samples (Crow and Condie, 1990); (c) post- Waterberg samples (Hanson et al., 2004b); (d) Mashonaland sill samples (Stubbs et al., 1999).

die (1990) and Klausen et al. (in press) were the only ones that measured Pb and these show positive Pb-anomalies which is a main difference to the dykes of this study.

Ti and V (Fig. 13 (a)) both behave incompatibly in basaltic tholeiites, with higher Ti and V concentrations in more evolved samples. Almost all samples plot between a Ti/V ratio of 20 and 50, which is typical for Ocean-Floor Basalts like MORBs; i.e., generated from a depleted mantle source. The more primitive ca. 1.87– 1.85 Ga dykes have slightly lower Ti/V-ratios, compared to most other data.

The Nb/Y and Zr/Y ratios in Fig. 13 (b) are not necessarily diagnostic of a certain tectonic setting but may be affected by differences in the petrogenesis and mantle source (Fitton et al., 1997). The less evolved ca. 1.87– 1.85 Ga and 2.7 Ga samples have lower Nb/Y and Zr/Y ratios but the differences are not very large. All of the 2.7 Ga samples plot along the base of Fitton et al's (1997) Icelandic array (i.e., $\Delta Nb < 0$), defined by Icelandic basalts with MgO > 5%. This is consistent with samples being derived from a slightly more depleted mantle source composition. In greater detail, the ca. 1.87– 1.85 Ga samples mostly plot at the border or within the array suggesting a composition more akin to an enriched Icelandic-type

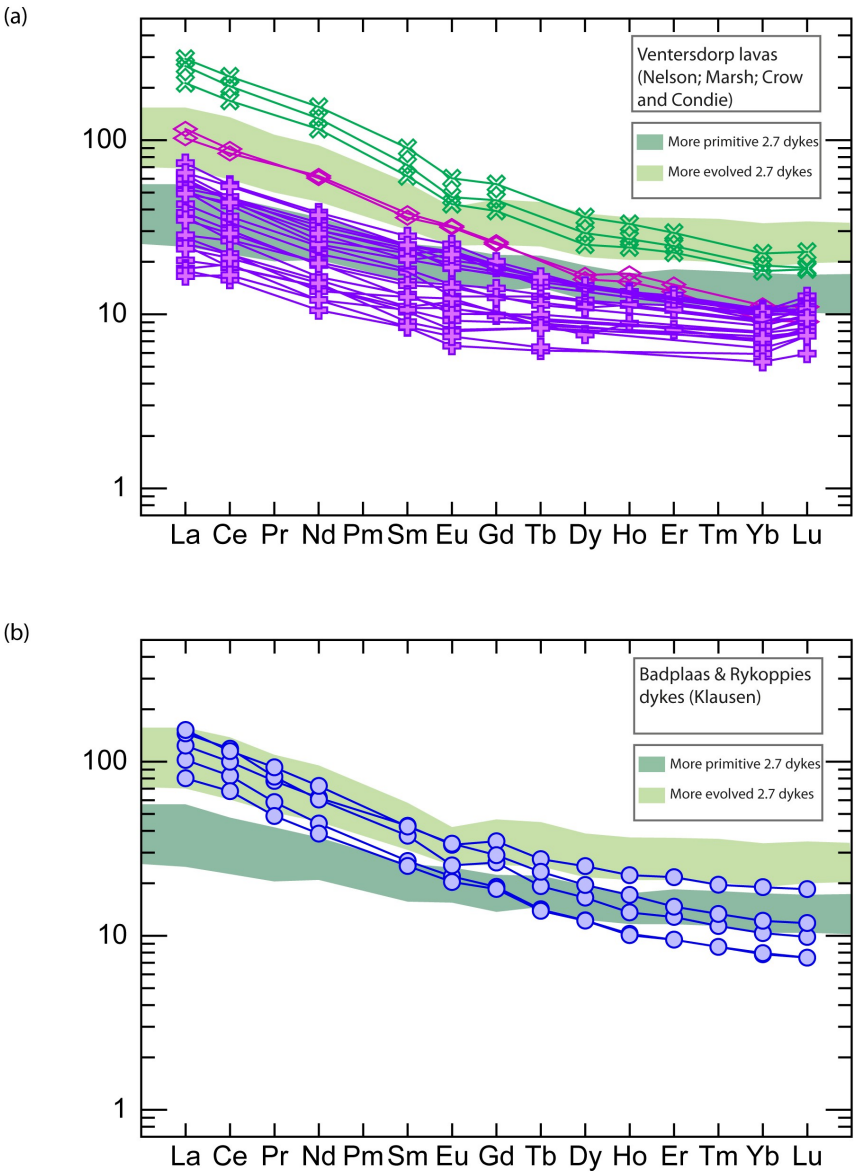

Figure 16. Chondrite normalised REE diagrams after Sun and MacDonough (1989) with shaded background representing the 2.7 Ga samples of this study for: (a) Ventersdorp lavas (Nelson et al., 1992; Marsh et al., 1992; Crow and Condie, 1988); (b) Rykoppies and Badplaas-Barberton dykes (Klausen et al., in press).

mantle source than the others. The post-Waterberg samples generally have slightly lower Nb/Y ratios than most of the Soutpansberg samples, the former of which could have either experienced a greater degree of crustal contamination or been derived by shallower depths of melting. The Ventersdorp lavas plot all under the array and show the lowest Nb/Y ratios of all. It seems that the Ventersdorp lavas are derived from a more depleted asthenospheric mantle source, because they might have been attributed to a mantle plume source. The Badplaas and Rykoppies dykes plot also under the array.

4.2.3. Rare earth elements (REE)

All of the plots in our chondrite normalised REE diagrams (Sun and MacDonough, 1989; Fig. 14) seem to be relatively parallel and LREE-enriched. This is a typical feature of continental tholeiites, derived from a more enriched mantle source and less typical for normal MORBs derived from a depleted mantle source. The REE slopes, determined as La/Lu ratios, are steeper in the more evolved samples. The less evolved 2.7 Ga samples (Fig. 14 (a)) show La/Lu ratios between 2.5 and 3.2, and the less evolved ca. 1.87– 1.85 Ga samples (Fig. 14 (c)) range between 2.3 and 3.0. In comparison the more evolved 2.7 Ga samples (Fig. 14 (b)), with a ratio between 3.4 and

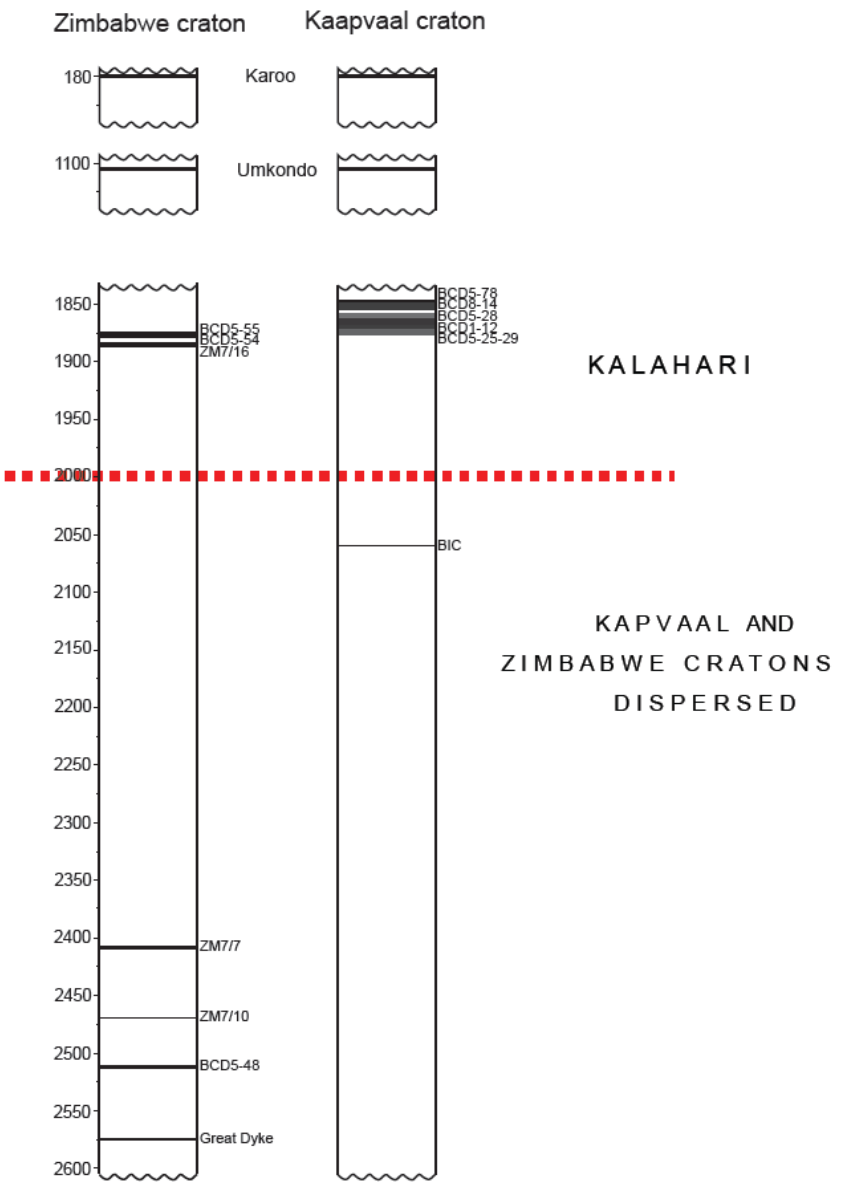

Figure 17. Barcode record of the Kaapvaal craton and Zimbabwe craton. Bar code matches at 0.18, 1.1 and at ca. 1.9 Ga infer a next-neighbour situation of the Zimbabwe and Kaapvaal cratons from ca. 2.0 Ga.

4.2, and the more evolved ca. 1.87– 1.85 Ga samples (Fig. 14 (d)), from 2.8 up to 3.7, have steeper profiles.

Most of the more evolved 2.7 Ga and ca. 1.87–1.85 Ga samples (Fig. 14 (b+d)) show slightly negative Eu- anomalies, whereas more primitive 2.7 Ga and ca. 1.87– 1.85 Ga samples do not. Very few of the more primitive samples even show slightly positive Eu- anomalies (e.g. BCD5-29, BCD5-30), which could be a sign of plagioclase accumulation. Otherwise, these differences in Eu- anomalies are more consistent with subsequent plagioclase fractionation rather than any residual plagioclase in a mantle source, located beneath a thick continental crust. Plagioclase fractionation is further substantiated by negative Eu-anomalies also becoming more prominent within the more evolved ca. 1.87– 1.85 Ga samples (Fig. 14 (d)). The slopes of the HREE of all the samples are very similar, as can be seen from Gd/Yb ratios ranging between 1.5 and 1.8, and may therefore indicate that these samples were generated from a similar source. The slopes of the LREE show larger differences, as shown by La/Sm ratios ranging between 2.0 and 4.3. The more evolved samples show higher La/Sm-ratios than less evolved samples of the same age, indicating that the LREE slopes changed during differentiation whereas the HREE did not.

The Soutpansberg lava samples (Fig. 15 (a)-(b)) are all LREE-enriched and some of these also show slightly negative Eu-anomalies; especially the ones from Bumby (2002). Eu-anomalies are more difficult to determine for the Crow and Condie (1990) samples because fewer REEs are published. The post - Waterberg samples (Fig. 15 (c)) and the Mashonaland sills (Fig. 15 (d)) are both LREE enriched but the post- Waterberg samples do not show negative Eu - anomalies like the Mashonaland sills.

Roughly coeval 2.7 Ga dykes from the Rykoppies and Badplaas- Barberton area (Klausen et al., in press) show mostly steeper and more elevated LREE profiles than the samples from this study. Furthermore, they exhibit steeper REE- profiles, compared to our 2.7 Ga intrusions. The Ventersdorp lavas (Fig. 16) are also generally LREE enriched. Within these lavas the Platberg Group show strong enrichments in REE and HFS

compared to the Klipriviersberg Group and the Allanridge Fm., whereas the Klipriviersberg Group has the lowest REE contents. The Platberg Group also shows minor negative Eu- anomalies. These feature are due to that the Platberg Group has the most evolved lavas here and has experienced more fractionation.

5. Discussion

5.1. Formation of the Kalahari craton

The Kalahari formed when the Kaapvaal and the Zimbabwe cratons collided and amalgamated into a single crustal unit. The timing of this collisional event, i.e. the formation of the Limpopo event, has been debated for considerable time (for review, see e.g. Mouri, 2008; Eriksson et al., 2008; and Zeh et al., 2010). Geochronology on metamorphic mineral assemblages within the Limpopo belt infers metamorphism both at 2.7 Ga and 2.0 Ga. While ages of 2.7 Ga are restricted to the Northern and Southern Marginal Zones of the Limpopo belt, the formation of new zircon is ubiquitous in the Central Zone of the belt. The older ages coincide in time with Ventersdorp magmatism, which originally was linked to NW-SE extension in response to NE-SW compression during the Kaapvaal- Zimbabwe collision (Light, 1982). However, Uken and Watkeys (1997) later favoured a link of the voluminous Ventersdorp magmatism to mantle plume activity.

More recent studies suggest the collision took place at 2.0 Ga during a granulite-grade event associated with large-scale folding in the Central Zone of the Limpopo belt (Mouri, 2008). The crust of the Central Zone was compressed and thickened in response to NNW-SSE shortening and was later changed to dextral transpressive tectonics along ENE trending structures (Holzer et al., 1998). The event of transpressive tectonics was associated with the age of peak metamorphism in the Limpopo Belt and then shifted to an extensional regime and dolerite intrusion some 100 Ma later, i.e. manifested by intrusion of 1.87 -1.85 Ga dykes investigated in this study.

High-precision geochronology of regional magmatic events in Zimbabwe and Kaapvaal can be used as an independent tool to bracket the timing of the collision between the two cratons (cf. Bleeker, 2003). In the north-east of the Bushveld Igneous Complex in the Kaapvaal craton NE trending dykes were dated at ca. 1.87-1.85 Ga for this study which are coeval with younger dolerite sheets (1879-1872 Ma) in the Waterberg Group (Hanson et al., 2004b) and, more importantly with the extensive Mashonaland event in Zimbabwe, recently dated at 1.89-1.87 Ga (Söderlund et al., in press). Besides a common event at ca. 1.9 Ga in the Kaapvaal and Zimbabwe cratons (Fig. 17), the barcodes show that magmatic activities of the same age took place at ca. 0.18 Ga (Jourdan et al., 2006) and at ca. 1.1 Ga (Hanson et al., 2004a). The lack of the Great Dyke (2.57 Ga) and Sebanga dyke ages (2.51 Ga, 2.47 Ga and 2.41 Ga) in the Kaapvaal craton and the corresponding lack of the Bushveld ages (2.06 Ga) in the Zimbabwe craton indicate that the two cratons were not in a next-neighbour situation from the late Archaean to the mid-Palaeoproterozoic. The 1.9 Ga event thus records the oldest event that is common in both cratons, hence suggesting that the formation of the Kalahari craton must have occurred prior to 1.9 Ga. It is here suggested that the Kalahari did not form until 2.0 Ga with reference to ages of metamorphic minerals in the Central Zone of the Limpopo belt. Older (ca. 2.7 Ga) ages recorded in the marginal zones of the Limpopo belt may indicate compressional active margin processes (i.e. subduction of oceanic crust) prior to the collision between Zimbabwe and Kaapvaal cratons.

5.2. Rotation-Post-1.87 Ga dextral shearing

The 1.89-1.87 Ga Mashonaland sills in the Zimbabwe craton are coeval with post-Waterberg sills and the here dated NE-trending Black Hills dykes in the Kaapvaal craton, with an additional slightly older magmatic pulse at ca. 1.93 Ga in Waterberg sediments (Hanson et al., 2004a). However, we note that the palaeomagnetic poles of these largely coeval units are significantly different (Michiel de Kock, 2007, Mushayandebvu et al., 1995). The difference in palaeomagnetic direction between coeval units suggest post-1.88 Ga relative motion between the cratons, i.e. shortly after the collisional event. This discordance in palaeomagnetic direction between the cratons can be explained by dextral strike-slip shearing along the Limpopo-bordering faults (David Evans, pers. comm., 2009). In fact, this scenario would be in perfect agreement with structural observations and kinematic indicators along shear zones bordering the Central Zone of the Limpopo belt (Mouri, 2008). An alternative explanation for the observed mismatch in palaeomagnetic directions requires consideration of unusually rapid apparent polar wander paths around 1.9 Ga.

The here proposed timing of events related to the formation of the Kalahari involves a main stage (>2.03 Ga) of crustal thickening of the Central Zone of the Limpopo during NNW–SSE shortening. From 2.03 to 2.01 Ga compressional tectonics shifted from orthogonal thrust tectonics to dextral transpressive tectonics along ENE trending structures, especially concentrated along shear zones adjacent to the Central Zone. Some 100 Ma later extensive magmas intruded, presumably as manifestation of orogenic collapse.

5.3. Petrogenesis

All of the samples have relatively low Mg numbers (18 -47), suggesting they do not represent primary melt. Additionally, other requirements for primary melts (Cr >1000 pm and Ni > 400-500 ppm; Winter, 2001) are not fulfilled by even the highest concentrations of 205 ppm Cr and 285 ppm Ni.

To figure out the depth of melt segregation, one may use incompatible trace element ratios like Zr/Nb (Fig. 18). According to Stubbs et al. (1999), this ratio is lower when partial melting takes place at deeper depths, as indicated by the modelled melting curves in Fig. 18 for primary melts. The trends defined by our dyke samples, which are not primary melt, cross the melting curves for even very low degrees of partial melting (~5%) of a depleted mantle, indicating that these magmas might be derived from a more enriched mantle source (probably located somewhere between DMM and BSE). The 2.7 Ga dykes seem to have evolved from slightly greater degrees of partial melting of such a mantle source. Roughly constant Zr/Nb ratios are just a little higher than the one of the

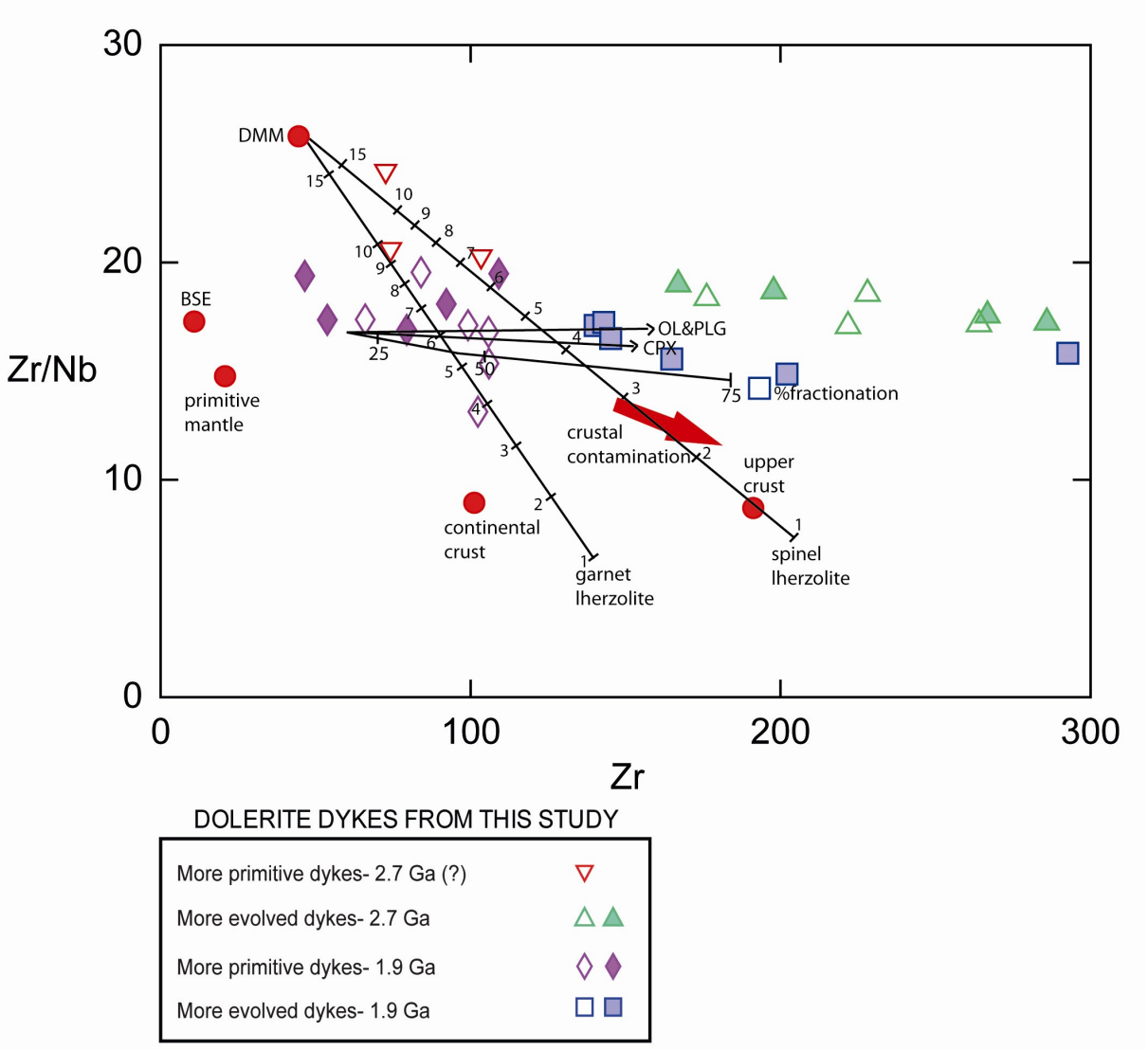

Figure 18. Zr/Nb vs. Zr diagram. Red dots indicate the compositions of primitive mantle (Taylor and McLennan, 1985), continental crust and upper crust (Sun and McDonough, 1989), bulk silicate earth (BSE) and depleted MORB mantle (DMM) (Kostopolous and James, 1992). Partial melting curves for garnet and spinel lherzolites (Schnetzler and Philpotts, 1970; Grutzeck et al., 1974) are calculated for the DMM. Fractionation of olivine (OL), plagioclase (PLG) and clinopyroxene (CPX) will shift compositions sub– horizontally towards higher Zr, by amount indicated by % fractionation.

primitive mantle and are more consistent with a more enriched mantle source (BSE). In general the depth of partial melting is hard to determine from this plot (mainly constructed for primary melts) because crystal fractionation and crustal contamination interferes.

Another possibility for the variation of Zr/Nb is crustal contamination, because crustal rocks generally have more distinctly negative Nb-anomalies. Thus, crustal contamination increases the Zr/Nb ratio just as higher degrees of partial melting also does. Thus, the slightly higher Zr/Nb ratio of the 2.7 Ga dykes could be explained by a slightly greater degree of crustal contamination as well as partial melting of a similar lherzolite source. It is also possible, however, that the primary melt for the 2.7 Ga dykes was derived from a more depleted source, lying somewhere between BSE and DMM in Figure 18.

Ti and V (Fig. 13 (a)) both behave incompatibly in basaltic tholeiites, with higher Ti and V concentrations in more evolved samples. Almost all samples plot between a Ti/V ratio of 20 and 50, which is typical for a MORB setting or Ocean-Floor Basalt, generated from a depleted mantle source. However, 2.7 Ga dykes plot towards slightly more alkaline Ti/V ratios, whereas (at least the primitive) ca. 1.87– 1.85 Ga dykes plot closer to more island-arc type ratios.

According to Fitton et al. (1997), the Nb/Y and Zr/V ratios in Fig. 13 (b) do not necessarily reflect a certain tectonic setting but may reflect differences in the petrogenesis and type of asthenospheric mantle source. A depleted mantle source is suggested for all of the 2.7 Ga samples and most of the ca. 1.87– 1.85 Ga samples that plot below the Icelandic array by Fitton et al. (1997). However, some ca. 1.87– 1.85 Ga

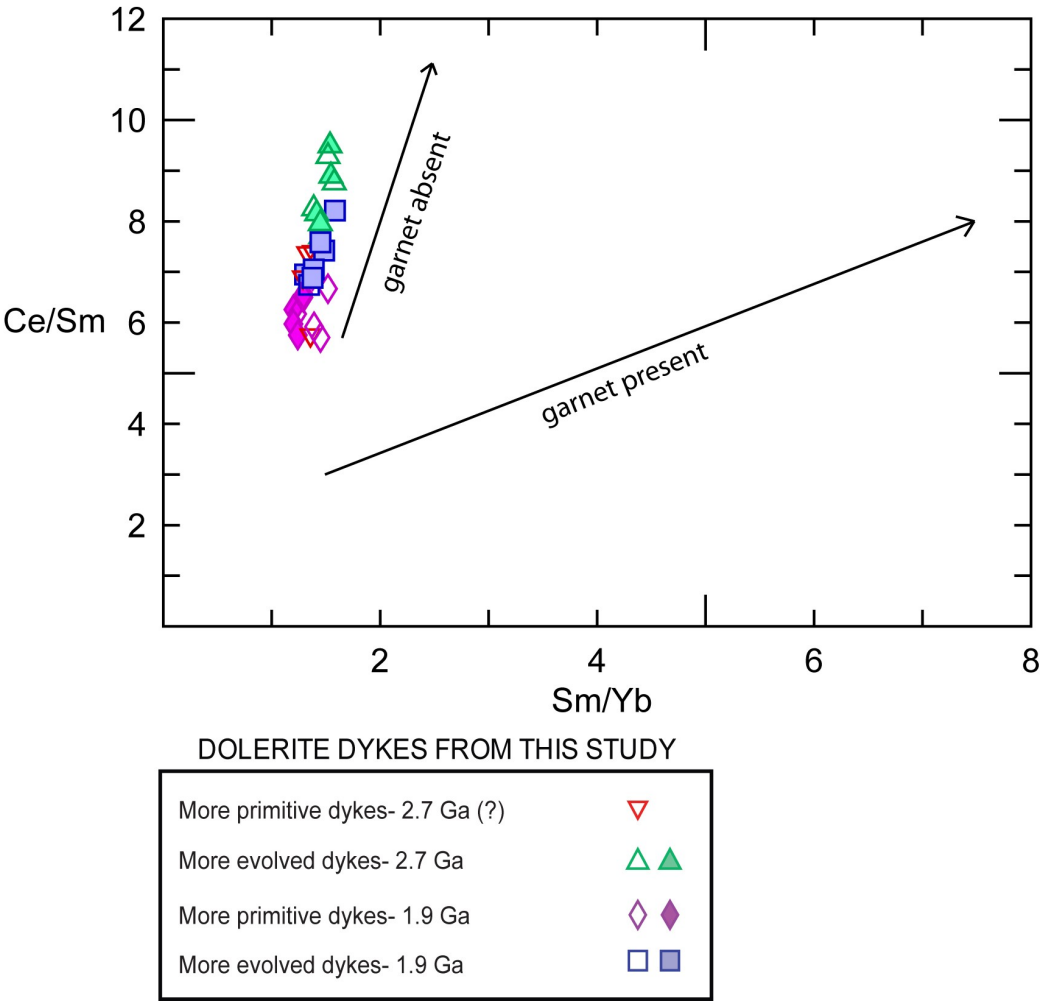

Figure 19. Ce/Sm vs. Sm/Yb diagram modified after Hawkesworth et al. (1984). The arrows point out to the presence/ absence of garnet as a residual phase in the source of the magmatism.

samples plot at the border or even within the array, suggesting that these compositions may be very slightly more akin to an enriched Icelandic-type mantle source. This is, not surprisingly, consistent with a similar interpretation made for Figure 18, based on a similar (Zr/Nb) ratio.

There seems to be no residual garnet in the magma source of these samples, indicating that it was not a deep magma source, because there is no significant HREE (e.g., Y-Yb) depletion. This can be illustrated by a Ce/Sm vs. Sm/Yb plot (Fig. 19) after Hawkesworth et al. (1984), where we see that all samples were not affected by residual garnet in the mantle source. This indicates that the magmas were produced in shallower depth above the garnet-lherzolite zone. Due to the little or no Eu-anomalies and the large crustal thickness of the Kaapvaal craton, melt segregation also occurred below the plagioclase lherzolite zone and the primary melts were therefore probably generated in the spinel lherzolite zone.

In general the major element trends are consistent with the fractionation of plagioclase and some Mg-rich phase. Furthermore, all samples also show a negative P-anomaly, which is indicative of apatite fractionation (Fig. 10). However, this apatite fractionation must have occurred and terminated early, during the differentiation of these magmas, in order for P_2O_5 to then increase with decreasing MgO.

Almost all of the dykes show TiO_2 values lower than 2 wt% and P_2O_5 lower than 0.5 wt%, which indicates that these dykes belong to the low P-Ti type, suggesting that primary magmas either were derived from a more depleted mantle source and/or affected by crustal contamination on the way towards the surface (Munyanyiwa, 1999).

There are greater differences among the LILE's in Fig. 10, which are more mobile and typically enriched through metasomatic processes (e.g., above subducting plates), thereby typically enriched in the continental crust that formed above subduction zones (Winter, 2001). There are no field relationships (e.g., syn- orogenic granites) that indicate that any of the mafic dyke swarms were emplaced close to any subduction zone setting, however. A subduction zone related setting is also difficult to reconcile with the intracratonic setting of both 2.7 Ga and ca. 1.87– 1.85 Ga intrusions and their more tholeiitic major element compositions. Thus, the enrichments in LILE are more likely due to either partial melting of a previously metasomatised sub-continental lithospheric mantle and/or

(a)

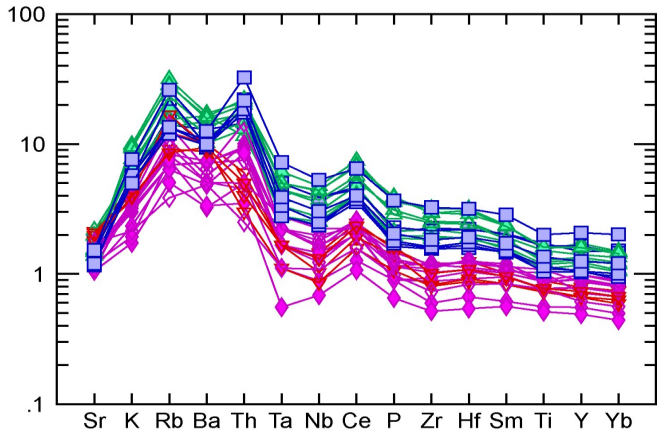

(b)

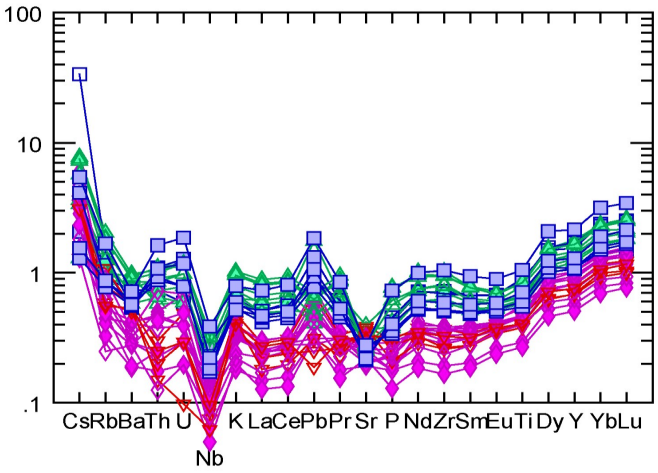

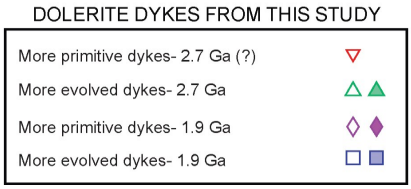

Figure 20. (a) MORB– normalised multi elements diagrams after Pearce (1983); (b) OIB – normalised multi elements diagrams after Sun and McDonough (1989).

crustal contamination.

The negative Nb-anomaly, together with the LILE- enrichment, is another subduction zone signature that can also be derived from either partial melting of a previously metasomatised SCLM and/or crustal contamination. The negative Pb-anomaly in primitive mantle normalised spider diagrams among the 2.7 Ga samples (Fig. 10) speaks also against a subduction zone setting. Subduction zone magmas usually show positive Pb-anomalies because Pb often forms within sulphide phases that are redeposited near the seawater crust and are usually break down by heat and dehydration during subduction, and thereby easily gets in the mantle wedge through hydrothermal fluids (Taylor and McLennan, 2009). The negative Nb-anomaly rather indicates crustal contamination, whereas the negative Pb-anomaly indicates that there was no active subduction zone activity. Similar 'subduction zone' signatures are often observed among most mafic igneous rocks from the Kaapvaal craton (e.g., Duncan 1984; Marsh 1984), and is thought to be an inherent chemical feature obtained from its sub-continental lithospheric mantle (Hawkesworth, 1984). Also the La/Nb ratios >1 are typical for continental flood basalts and variable degrees of crustal contamination (Munyanyiwa, 1999) and suggest a more intra-continental setting.

MORB normalised spider diagrams (Fig. 20 (a)) show LILE enrichments and slightly negative Ta-Nb anomalies which are usually a feature for subduction zones. The high LILE and HFSE contents are features of many intra-continental volcanics (Fitton et al., 1988, Hawkesworth et al., 1990) supposing a depleted mantle source that has been LILE- enriched. This is typical for a SCLM source which could have been caused by effects of earlier subduction processes (Winter, 2001). The OIB normalised spider diagrams (Fig. 20 (b)) show a positive slope from P to Lu indicating a more depleted mantle source. Negative Nb anomalies could be caused by fluid enrichment of the crust or the mantle source.

The correspondence analysis of the samples (Fig. 5) show some geochemical differences between

the groups. The F2 variation is mainly controlled by fractionation processes. It shows that the more incompatible and evolved dykes have lower F2 whereas the more primitive dykes have F2>0 values. Variations within the HFSE/LILE and HREE/LREE ratios, on the other hand, seems to control F1 values. Thus, the 2.7 Ga dykes are more enriched in LILE and LREE, shown by F1>0, whereas the ca. 1.87– 1.85 Ga dykes have values F1<0.

The 2.7 Ga dykes from this study are significantly different from 2.7 Ga dykes emplaced farther south. Like the ca. 1.87– 1.85 Ga dykes, they show a more tholeiitic basalt character with lower LILE and shallower REE profiles. The ca. 1.87– 1.85 Ga dykes could be emplaced in a continental (back-arc) rift setting (Klausen et al., in press) that might be consistent with some geochemical features, e.g. like negative (Nb, Ta)- anomalies. But the involvement of a metasomatised sub-continental lithospheric mantle source is needed, which is unique for individual cratons (Duncan, 1987; Marsh, 1987). It is also possible that these lithospheric melts were variably mixed in with primary basaltic melts from an asthenospheric mantle source, as advocated for 0.18 Ga Karoo magmas (Jourdan et al., 2007). This model might explain slight differences between ca. 1.87– 1.85 Ga and 2.7 Ga dykes from this study, as well as the larger differences between coeval 2.7 Ga dykes of this study (NE- trending) and more southerly ones (Klausen et al., in press) which could reflect differences in the SCLM below the northern and southern part of the eastern Kaapvaal. Ca. 1.87– 1.85 Ga dykes were probably derived from a slightly more asthenospheric and less metasomatised mantle source compared to sub- parallel 2.7 Ga dykes.

6. Conclusion

Baddeleyite U-Pb dates of five NE trending dykes located NE of the Bushveld Igneous Complex in the Kaapvaal craton range between 1.85 Ga and 1.87 Ga. They are thus coeval with younger dolerite sheets (1.88-1.87 Ga) in the Waterberg Group (Hanson et al., 2004b) and with the Mashonaland sills (1.89-1.87 Ga) in the Zimbabwe craton (Söderlund et al., in press). These ages record the oldest common event in both cratons suggesting a formation age of the Kalahari craton prior to 1.87 Ga. The absence of Sebanga dyke ages (2.41, 2.47 and 2.51 Ga) and Great Dyke ages (2.6 Ga) in Kaapvaal and the corresponding absence of BIC (2.06 Ga) and other pre-2.0 Ga ages of dykes in Zimbabwe infers the Kalahari craton did not formed until ca. 2.0 Ga, in accordance with radiometric ages of metamorphic minerals in the Central Zone of the Limpopo belt.

The palaeomagnetic poles of the Mashonaland sills, the post-Waterberg sills and the NE-trending dykes in the Kaapvaal craton are close, though significantly different, which suggests post-1.88 Ga motion between the cratons, i.e. shortly after the collisional event (M. de Kock, U. of Johannesburg, pers. comm., 2009). This discrepancy can be explained by dextral strike-slip shearing along the Limpopo-bordering faults in accordance with structural evidence (D. Evans, U. of Berkely, pers. comm., 2009).

Geochemically, the samples are not representing primary melt due to low Mg numbers and low Cr and Ni content. The magma source does not seem to be neither garnet- nor plagioclase peridotite, but rather these magmas represent partial melting of spinel-bearing peridotite. The LILE enrichments and negative Nb- anomalies are typical subduction zone features but are here more likely to originate from either partial melting of a previously metasomatised sub-continental lithospheric mantle and/or crustal contamination. The ca. 1.87– 1.85 Ga dykes might be emplaced in a continental rift setting or a continental back- arc setting requiring a metasomatised lithosperic mantle source, possibly mixed in by primary basaltic melts from an asthenospheric mantle source. The NE- trending 2.7 Ga dykes are significantly different from 2.7 Ga dykes emplaced farther south with other trends and show more tholeiitic basaltic character like the ca. 1.87– 1.85 Ga dykes. However, NE-trending ca. 1.87– 1.85 Ga dykes may still have been derived from a asthenospheric and less metasomatised mantle source, relative to the sub-parallel 2.7 Ga dykes.

- Melts were generated at relatively shallow depths (spinel stability field) and experienced plagioclase, Mg- rich phases and apatite fractionation
- No significant geochemical differences between 2.7 Ga and 1.9 Ga dykes → similar petrogenetic origins
- These ages record the oldest common event in the Kaapvaal and Zimbabwe craton → suggesting formation of the Kalahari craton at ca 2.0 Ga rather than 2.7 Ga
- Baddeleyite U-Pb ages of 5 dykes within the Black Hills swarm were dated yielding emplacement ages in the range 1.87- 1.85 Ga, which make this swarm coeval with post-Waterberg sills and the Mashonaland sill complex

Acknowledgements

I would like to thank my supervisor Ulf Söderlund for all his support during the work on this project and my co-supervisors Johan Olsson and Martin Klausen for their efforts and time. A special thanks to my family for supporting me and believing in me the whole time. Finally, thanks to my friends who made an effort to help me or just listen to me and put things in their right perspective.

References

Armstrong, R.A., Compston, W., Retief, E.A., Williams, I.S., Welke, H.J., 1991: Zircon ion microprobe studies bearing on the age and evolution of the Witwatersrand triad. *Precambrian Research 53*, 243-266.

Barton, J. M., 1979: The chemical compositions, Rb-Sr isotopic systematics and tectonic setting of certain post-kinematic mafic igneous rocks, Limpopo Mobile Belt, southern Africa. *Precambrian Research 9*, 57–80.

Barton Jr., J.M., Blignaut, E., Salnikova, E.B., Kotov, A.B., 1995: The stratigraphical position of the Buffelsfontein Group based on field relationships and chemical and geochronological data. *South African Journal of Geology 98*, 386-392.

Benzecri, J. -P. ,1992: *Correspondence analysis handbook*. New York: Marcel Dekker.

Beukes, N.J. and Cairncross, B., 1991: A lithostratigraphic-sedimentological reference profile for the Late Archaean Mozaan Group, Pongola Sequence: application to se quence stratigraphy and correlation with the Witwatersrand Supergroup. *South African Journal of Geology 94*, 44-69.

Berger, M., Kramers, J.D., Nägler, T.F., 1995: Geochemistry and geochronology of charnoenderbites in the Northern Marginal Zone of the Limpopo Belt, Southern Africa, and genetic models. *Schweizerische Mineralogische und Petrographische Mitteilungen 75*, 17-42.

Bleeker, W., 2003: The later Archean record: a puzzle in ca. 35 pieces. *Lithos 970*, 99-134.

Brandl, G., Cloete, M., Anhaeusser, C.R., 2006: Archaean greenstone belts. In: Johnson, M.R., Anhaeusser C.R., Thomas, R.J. (Eds.), *The geology of South Africa. Geological Society of South Africa*. Johannesburg/ Council for Geoscience, Pretoria, pp. 691.

Buick, I.S., Maas, R., Gibson, R., 2001: Precise U-Pb titanite age constraints on the emplacement of the Bushveld Complex, South Africa. *Journal of the Geological Society, London 158*, 3-6.

Bumby, A.J., Eriksson, P.G., van der Merwe, R., Maier, W.D., 2001: The stratigraphic relationship between the Waterberg and Soutpansberg Groups in Northern Province, South Africa: Evidence from the Blouberg area, *South African Journal of Geology 104*, 205-216.

Bumby, A.J., Eriksson, P.G., van der Merwe, R., Steyn, G.L., 2002: A halfgraben setting for the Proterozoic Soutpansberg Group (South Africa): evidence from the Blouberg area. *Sedimentary Geology 147*, 37-56.

Burke, K., Kidd, W.S.F., Kusky, T.M., 1985: The Pongola structure of southeastern Africa: The world's oldest preserved rift?. *Journal of geodynamics 2*, 35-49.

Button, A., 1981: The Pongola Supergroup. In: Hunter, D.R. (Ed.), *Precambrian of the Southern Hemisphere*. Elsevier, Amsterdam, 501–510.

Cawthorn, R.G., Eales, H.V., Walraven, F., Uken, R., Wat keys, M.K., 2006: The Bushveld Complex. In: Johnson, M.R., Anhaeusser C.R., Thomas, R.J. (Eds.), *The geology of South Africa*. Geological Society of South Africa. Johannesburg/Council for Geoscience, Pretoria, 691 p.

Clausen, S. -E., 1998): *Applied correspondence analysis: An introduction.* Thousand Oaks, CA: Sage Publications.

Crow, C. and Condie, K.C., 1988: Geochemistry and origin of late Archean volcanics from the Ventersdorp Supergroup, South Africa. *Precambrian Research, 42*.

Crow, C. and Condie K.C., 1990: Geochemistry and origin of early Proterozoic volcanic rocks from the Transvaal and Soutpansberg successions, South Africa. *Precambrian Research 47*, 17-26.

Davis, J.C., 2002: *Statistics and Data Analysis in Geology. 3rd edition.* New York: John Wiley, 656 p.

de Wit, J.M., Roering, C., Hart, R.J., Armstrong, R.A., De Ronde, C.E.J., Green, R.W.E., Tredoux, M., Peberdy, E., Hart, R.A., 1992: Formation of an Archean continent. *Nature 357*, 553-562.

de Kock, M.O., 2007: Paleomagnetism of selected Neoachean-Paleoproterozoic cover sequences on the Kaapvaal craton and implications for Vaalbara. Unpublished Ph.D. Thesis. University of Johannesburg, Johannesburg, 276 p.

Duncan, A.R., 1987: The Karoo igneous province– a problem area for inferring tectonic setting from basalt geochemistry. In: S.D. Weavers and R.W. Johnson (Eds.), *Tectonic Controls on Magma Chemistry.* Journal of Volcanology and Geothermal Research 32, 13– 34.

Duncan, A.R., Erlank, A.J. and Marsh, J.S., 1984: Regional geochemistry ofthe Karoo igneous province. *Geological Society of South Africa, Spec. Publ., 13,* 355-388.

Eglington, B.M. and Armstrong, R.A., 2004: The Kaapvaal Craton and adjacent orogens, southern Africa: a geochronological database and overview of the geological development of the craton. *South African Journal of Geology 107*, 13-32.

Eriksson, P.G. and Altermann, W., 1998: An overview of the geology of the Transvaal Supergroup dolomites (South Africa). *Environmental Geology 36 (1-2)*, 179-188.

Eriksson, P.G., Altermann, W., Catuneanu, O., van der Merwe, R., Bumby, A.J., 2001: Major einfluences on the evolution of the 2.67– 2.1 Ga Transvaal basin, Kaapvaal craton. *Sedimentary Geology 141– 142*, 205-231.

Eriksson, P.G., Condie, K.C., van der Westhuizen, W., van der Merwe, R., de Bruiyn, H., Nelson, D.R., Altermann, W., Catuneanu, O., Bumby, A.J., Lindsay, J., Cunningham, M.J., 2002: Late Archean superplume events: a Kaapvaal-Pilbara perspective. *Journal of Geodynamics 34*, 207-247.

Eriksson, P.G., Altermann, W., Hartzer, F.J., 2006: The Transvaal Supergroup and its precursors. In: Johnson, M.R., Anhaeusser C.R., Thomas, R.J. (Eds.), *The geology of South Africa.* Geological Society of South Africa. Johan - nesburg/Council for Geoscience, Pretoria, 691 p.

Eriksson, P.G., Banerjee, S., Nelson, D.R., Rigby, M.J., Catuneanu, O., Sarkar, S., Roberts, R.J., Ruban, D., Mtimkulu, M.N., Raju, P.V.S., 2008: A Kaapvaal craton debate: Nucleus of an early small supercontinent or affected by an enhanced accretion event?. *Gondwana Research, 15, Issues 3-4*, 354-372.

Ernst, R.E., Head, J.W., Parfitt, E., Grosfils, E., Wilson, L., 1995: Giant radiating dyke swarms on Earth and a Venus. *Earth Science Reviews 39*, 1-58.

Ernst, R.E., Buchan, K.L., 2001: Large mafic magmatic events through time and links to mantle-plume heads. In: Ernst, R.E., and Buchan, K.L., (Eds.) Mantle Plumes: Their Identification Through Time. *Geological Society of America Special Paper 352*, 483-575.

Fitton, J.G., James, D., Kempton, P.D., Ormerod, D.S., Leeman, W.P., 1988: The role of lithospheric mantle in the generation of late cenozoic basic magmas in the western United States. *Journal of Petrology Special Volume 1,* 331-349.

Fitton, J.G., Saunders, A.D., Norry, M.J., Hardarson, B.S., Taylor, R.N., 1997: Thermal and chemical structure of the Iceland plume. *Earth and Planetary Science Letters 153*, 197-208.

Greenacre, M. J.1, 984: *Theory and applications of correspondence analysis*. New York: Academic Press.

Greenacre, M. J., 1993: *Correspondence analysis in practice*. London: Academic Press.

Grutzeck,M, Kridelbaugh, S., Weill, D.F., 1974: The distribution of Sr and REE between diopside and silicate liquid. *Geophysical Research Letters 1*, 273– 275.

Hanson, R.E., Crowley, J.L., Bowring, S.A., Ramezani, J., Gose, W.A., Dalziel, I.W.D., Pancake, J.A., Seidel, E.K., Blenkinsop, T.G., Mukwakwami, J., 2004a: Coeval large-scale magmatism in the Kalahari and Laurentian cratons during Rodinia assembly. *Science 304*, 1126-1129.

Hanson, R.E., Gose, W.A., Crowley, J.L., Ramezani, J., Bowring, S.A., Bullen, D.S., Hall, R.P., Pancake, J.A., Mukwakwami, J., 2004b: Paleoproterozoic intraplate magmatism and basin development on the Kaapvaal

Craton: Age, palaeomagnetism and geochemistry of ~1.93 to ~1.87 Ga post-Waterberg dolerites. *South African Journal of Geology 107*, 233-254.

Hawkesworth, C.J., Marsh, J.S., Duncan, A.R., Erlank, A.J., and Norry, M.J., 1984: The role of continental lithosphere in the generation of the Karoo volcanic rocks: evidence from combined Nd and Sr-isotope studies. *Special Publication of the Geological Society of South Africa, v. 13*, p. 341-354.

Hawkesworth, C.J., Kempton, P.D., Rogers, N.W., Ellam, R.M., van Calsteren, P.W., 1990: Continental mantle lithosphere, and shallow level enrichment processes in the Earth's mantle. *Earth and Planetary Science Letters 96*, 256-268.

Heaman, L., LeCheminant, A.N., 1993: Paragenesis and U-Pb systematics of baddeleyite (ZrO_2). *Chemical Geology 119*, 95-126.

Holzer, L., Frei, R., Barton, J. M., Jr & Kramers, J. D.,1998: Unraveling the record of successive high grade events in the Central Zone of the Limpopo Belt using Pb single phase dating of metamorphic minerals. *Precambrian Research 87*, 87-115.

Hunter, D.R. and Reid, D.L., 1987: Mafic dyke swarms in southern Africa. In: *Mafic Dyke Swarms.* Edited by Halls, H.C. and Fahrig, W.F., Geological Association of Canada 34, 445-456.

Hunter, D.R. and Halls, H.C., 1992: A geochemical study of a Precambrian mafic dyke swarm, Eastern Transvaal, South Africa. Journal of African Earth Sciences 15, 153 - 168.

Irvine, T. N. and Baragar, W. R. A., 1971: A guide to the chemical classification of the common volcanic rocks. *Canadian Journal of Earth Science 8*, 523-548.

Jacobsen, J.B.E., Rix, D.C., Sevensten, W.J., 1975: K-Ar Ages of some Mafic Dykes from the Messina District, Transvaal, and their Bearing on the Age of Copper Mineralization. *Geological Society of South Africa Transactions 78*, 359-360.

Jaeckel, P., Kröner, A., Kamo, S.L., Brandl, G.,Wendt, J.I., 1997: Late Archaean to Early Proterozoic granitoid magmatism and high grade metamorphism in the central Limpopo belt, South Africa. *Journal of the Geological Society of London 154*, 25–44.

James, D.E., Niu, F., Rokosky, J., 2003: Crustal structure of the Kaapvaal craton and its significance for early crustal evolution. *Lithos 71*, 413-429.

Jansen, H., 1976: The Waterberg and Soutpansberg Groups in the Blouberg area, northern Transvaal. *Transactions geological Society South Africa 79*, 281-291.

Jourdan, F., Féraud, G., Bertrand, H., Watkeys, M.K., Kam punzu, A.B., Le Gall, B., 2006: Basement control on dyke distribution in Large Igneous Provinces: Case study of the Karoo triple junction. *Earth and Planetary Science Letters 241*, 307-322.

Klausen, M.B., Söderlund, U., Olsson, J.R., Ernst, R.E., Armoogam, M., Mkhize, S.W., Petzer, G. Petrological discrimination among Precambrian dyke swarms; Eastern Kaapvaal craton (South Africa), *Precambrian Research* (in press).

Kostopoulos, D.K., James, S.D., 1992: Parameterization of the melting regime of the shallow upper mantle and the affects of variable lithospheric stretching on mantle modal stratification and trace element concentrations in magmas. *Journal of Petrology 33,* 665– 691.

Kreissig, K., Holzer, L., Frei, R., Villa, I.M., Kramers, J.D., Kröner, A., Smit, C.A., Van Reenen, D.D., 2001: Geochronology of the Hour River Shear Zone and the metamorphism in the Southern Marginal Zone of the Limpopo belt, Southern Africa, *Precambrian Research 109*, 145-173.

Kröner, A. and Compston, W., 1988: Ion microprobe ages of zircons from early Archean granite pebbles and greywacke, Barberton Greenstone Belt, Southern African *Precambrian Research 38*, 367-380.

LeBas, M.J., LeMaitre, R.W., Streckeisen, A.L., Zanettin, B., 1986: A chemical classification of volcanic rocks based on the total- alkali- silica diagram. *Journal of Petrology 27*, 745-750.

Lee, C.A., 1996: A review of mineralization in the Bushveld Complex and some other layered intrusions. In: Cawthorn R.G. (Ed.), *Layered intrusions.* Amsterdam, Elsevier Science B.V., 103-145.

Letts, S., Torsvik, T.H., Webb, S.J., Ashwal, L.D., Eide, E.A., Chunnett,G., 2005: Palaeomagnetism and $^{40}Ar/^{39}Ar$ geochronology of mafic dykes from the eastern Bushveld Complex (South Africa). *Geophysical Journal International 162*, 36-48.

Light, M.P.R., 1982: The Limpopo Mobile Belt: A result of continental collision. *Tectonics 1 (4)*, 325-342.

Luais, B. & Hawkesworth,C. J. 1994: The generation of continental crust; an integrated study of crust-forming processes in the Archaean of Zimbabwe. *Journal of Petrology, 35*, 45-93.

Ludwig, K. R., 2003: *User's manual for Isoplot 3.00: A geo chronological toolkit for Microsoft Excel*. Berkeley Geochronology Center, Special Publication 4, 71 p.

MacDonough, W.F. and Sun, S. -s., 1995: The composition of the Earth. *Chemical Geology 120*, 223– 254.

Mapeo, R.B.M., Arnstrong, R.A., Kampunzu, A.B., Modisi, M.P., Ramokate, L.V., Modie, B.N.J., 2006: A ca. 200 Ma hiatus between the Lower and Upper Transvaal Groups of southern Africa: SHRIMP U- Pb detrital zircon evidence from the Segwagwa Group, Botswana: Implications for Palaeoproterozoic glaciations. *Earth and Planetary Science Letters 244*, 113-132.

Marsh, J.S. and Eales, H.V., 1984: Chemistry and petrogenesis of the igneous rocks of the Karoo central area, southern Africa. *Geological Society of South Africa, Special Publication 13,* 27- 68.

Marsh, J.S., 1987: Basalt geochemistry and tectonic discrimination within continental flood basalt provinces. In: S.D. Weavers and and R.W. Johnson (Eds.), *Tectonic Controls on Magma Chemistry*. Journal of Volcanology and Geothermal Research 32, 35-49.

Marsh, J.S., Bowen, M.P., Rogers, N.W., Bowen, T.B., 1992: Petrogenesis of late Archaean flood-type basic lavas from the Klipriviersberg Group, Ventersdorp Supergroup, South Africa. *Journal of Petrology 33*, 817–847.

Mouri, H., Brandl, G., Whitehouse, M., de Waal, S., Guiraud, M., 2008: CL-imaging and ion microprobe dating of single zircons from a high-grade rock from the Central zone, Limpopo belt, South Africa: evidence for a single metamorphic event at ~2.0 Ga. *Journal of African Earth Sciences 50*, 111-119.

Munyanyiwa, H., 1999: Geochemical study of the Umkondo dolerites and lavas in the Chimanani and Chipinge Districts (eastern Zimbabwe) and their regional implications. *Journal of African Earth Sciences, Vol. 28 (2)*, 349-365.

Mushayandebvu, M.F., Bates, M.P., Jones, D.L., 1995: Ani sotropy of magnetic susceptibility results from the Mashonaland dolerite sills and dykes of northeast Zimbabwe. *Physics and Chemistry of Dykes,* Baeer & Heimann (Eds.), Balkema, Rotterdam, 151-161.

Nelson, D.R., Trendall, A.F., de Laeter, J.R., Grobler, N.J., Fletcher, I.R., 1992: A comparative study of the geochemical and isotopic systematics of Late Archaean flood basalts from the Pilbara and Kaapvaal Cratons. *Precambrian Res., 54*, 231-256.

Nisbet, E. G., Bickle, M. J. & Martin, A., 1977: The mafic and ultramafic lavas of the Belingwean Greenstone Belt, Rhodesia. *Journal of Petrology 18*, 521-566.

Oberthür, T., Davis, D.W., Blenkinsop, T.G., Höhndorf, A., 2002: Precise U-Pb mineral ages, Rb-Sr and Sm-Nd systematics for the Great Dike, Zimbabwe–constraints on late Archean events in the Zimbabwe craton and Limpopo belt. *Precambrian Research 113*, 293-305.

Olsson, J.R., Söderlund, U., Klausen, M.B., Ernst, R.E., this volume. U-Pb baddeleyite ages of major Archean dike swarms and the Bushveld Complex, Kaapvaal Craton

(South Africa); correlations to volcanic rift forming events. *Precambrian Research* (this volume).
Pearce, J.A., 1996: A user's guide to basalt discrimination diagrams. In: Bailes (Ed.), *Trace element geochemistry of volcanic rocks; applications for massive sulphide exploration, Short Course Notes.* Geological Association of Canada 12, 79-113.
Poujol, M., Robb, L.J., Respaut, J.P., Anhaeusser, C.R., 1996: 3.07– 2.97 Ga greenstone belt formation in the northeastern Kaapvaal craton: implications for the origin of the Witwatersrand basin. *Economic Geology 91 (8),* 1455-1461.
Robb, L.J. and Meyer, F.M., 1995: The Witwatersrand Basin, South Africa: geological framework and mineralization processes. *Ore Geol. Rev. 10*, 67-94.
Rollinson, H.R., 1993: *Using geochemical data: Evaluation, presentation, interpretation.* John Wiley & Sons, Inc., New York. 352 p.
Schnetzler, C.C., Philpotts, J.A., 1970: Partition coefficents of rare earth elements between igneous matrix material and rock forming mineral phenocrysts– II. *Geochimica Cosmochimica Acta 34*, 331– 340.
Sharpe, M.R., 1981: The chronology of magma influxes to the eastern compartment of the Bushveld Complex as exemplified by its marginal border groups. *Journal of the Geological Society of London 138*, 307-326.
Shervais, J.W., 1982: Ti– V plots and the petrogenesis of modern and ophiolitic lavas. *Earth and Planetary Science Letters 59,* 101– 118.
Söderlund, U., Johansson, L., 2002: A simple way to extract baddeleyite (ZrO2). Geochemisty Geophyics Geosystematics 3 (2), 1014.
Söderlund, U., Elming, S.-Å., Ernst, R.E. and Schissel, D., 2006: The Central Scandinavian Dolerite Group- Protracted hotspot activity or back-arc magmatism? Constraints from U-Pb baddeleyite geochronology and Hf isotopic data. *Precambrian Research 150*, 136–152.
Söderlund, U., Hofmann, A., Klausen, M.B., Olsson, J.R., Ernst, R.E. Towards a complete magmatic barcode for the Zimbabwe craton: Baddeleyite U-Pb dating of regional dyke swarms and sill complexes. *Precambrian Research* (this volume).
Stacey, J.S., Kramers, J.D., 1975: Approximation of Terrestrial lead isotope evolution by a two– stage model. *Earth and Planetary Science Letters 26*, 207– 221.
Stanistreet, I.G., McCarthy, T.S., 1991: Changing tectonosedimentary scenarios relevant to the development of the late Archean Witwatersrand Basin. *Journal of African Earth Sciences 13*, 65-82.
Strik, G., de Wit, M.J., Langereis, C.G., 2007: Palaeomagnetism of the Neoarchaean Pongola and Ventersdorp Supergroups and an appraisal of the 3.0- 1.9 Ga apparent polar wander path off the Kaapvaal Craton, South Africa. *Precambrian Research 153*, 96-115.
Stubbs, H.M., Hall, R.P., Hughes, D.J., Nesbitt, R.W., 1999: Evidence for a high Mg andesitic parental magma to the East and West satellite dikes of the Great Dike, Zimbabwe: a comparison with the continental tholeiitic Mashonaland sills. *Journal of African Earth Sciences 28*, 325-336.
Stubbs, H.M., 2000: The *geochemistry* and *petrogenesis* of the Archaean and Palaeoproterozoic dykes and sills of *Zimbabwe*. PhD thesis. University of Portsmouth, 340 p.
Sun, S. -s., MacDonough, W.F., 1989: Chemical and isotopic systematic of ocean basalts: implications for mantle composition and processes. In: Saunders, A.D., Norry, M.J. (eds), *Magmatism in oceanbasins*. Geology Society of London Special Publication 42, 313– 345.
Taylor, S.R., McLennan, S.M., 1985: The Continental Crust: its composition and evolution. *Blackwell Scientific Publications*, 312pp.
Taylor, S.R., McLennan, S.M., 2009: *Planetary Crusts: Their Composition, Origin and Evolution.* Cambridge University Press. 400 p.
Uken, R. and Watkeys, M.K., 1997. An interpretation of mafic dyke swarms and their relationship with major mafic magmatic events on the Kaapvaal Craton and Limpopo Belt. *South African Journal of Geology 100*, 341-348.
Wilson, J.F., Jones, D.L., Kramers, J.D., 1987: Mafic dike s warms in Zimbabwe. In: Halls H.C. and Fahrig, W.F. (Eds.), *Mafic dike swarms*. Geological Association of Canada, Special paper Dike Swarms. Spec. Pap. Geol. Ass. Can. 34, 433-444.
Wilson, J.F., Nesbitt,R.W. & Fanning,C.M., 1995: Zircon geochronology of Archaean felsic sequences in the Zimbabwe craton: a revision of greenstone stratigraphy and a model for crustal growth. In: Coward,M.P. & Ries, A.C. (Eds.), *Early Precambrian Processes*. Geological Society Special Publication No. 95, 109-126.
Winter, J.D., 2001: *An Introduction to Igneous and Metamorphic Petrology*. Prentice- Hall. Inc., 697 p.
Zeh, A., Gerdes, A., Klemd, R., Barton, Jr, J.M., 2007: Archaean to Proterozoic crustal evolution in Central Zone of the Limpopo Belt (South Africa-Botswana): Constraints from combined U-Pb and Lu-Hf isotope analyses of zircon. *Journal of Geology 104*, 13-22.
Zeh, A., Gerdes, A., Barton Jr., J., Klemd, R., 2010: U-Th-Pb and Lu-Hf systematics of zircon from TTG's, leucosomes, metaanorthosites and quartzites of the Limpopo Belt (South Africa): constraints for the formation recycling and metamorphism of Palaeoarchaean crust. *Precambrian Research 170*, 50-68.

Appendix 1: Major and Trace element ICP-Ms analyses

Sample	BCD1-12	BCD1-13	BCD1-15	BCD1-17	BCD1-18	BCD1-19	BCD1-21	BCD1-22	BCD5-21	BCD5-22	BCD5-23	BCD5-25	BCD5-26	BCD5-27	BCD5-28
Major elements (wt%)															
SiO_2	50.25	47.78	49.27	46.65	48.48	48.99	50.34	48.73	48.52	50.4	50.58	49.65	50.08	49.71	49.01
Al_2O_3	15.01	15.79	13.2	15.68	12.66	13.45	13.89	14.64	14.85	13.39	13.15	14.88	14.62	14.01	14.7
Fe_2O_3	13.96	13.99	16.43	13.43	17.6	16.27	14.14	14.66	14.85	16.59	16.63	10.7	13.58	15.2	13.88
MgO	5.22	6.37	4.68	7.69	4.99	5.07	6.75	6.93	6.64	4.71	4.28	9.41	6.34	5.25	7.3
CaO	9.19	9.26	8.82	10.18	9.15	9.01	10.49	10.16	10.17	8.93	8.22	11.15	10.09	9.22	10.42
Na_2O	2.77	2.55	2.55	2.18	2.3	2.5	2.15	2.22	2.29	2.63	2.65	1.71	2.33	2.47	2.25
K_2O	0.93	0.7	0.92	0.5	0.82	0.89	0.45	0.48	0.54	1.05	1.48	0.26	0.51	0.99	0.35
TiO_2	1.66	1.32	2.27	1.53	2.58	1.78	1.15	1.16	1.3	1.91	2.32	0.84	1.34	1.65	1.31
P_2O_5	0.2	0.19	0.38	0.18	0.26	0.24	0.11	0.11	0.14	0.26	0.44	0.11	0.14	0.23	0.14
MnO	0.19	0.18	0.21	0.18	0.23	0.2	0.2	0.2	0.2	0.21	0.2	0.17	0.19	0.19	0.2
LOI	0.3	1.6	1	1.5	0.6	1.3	0	0.4	0.2	-0.4	-0.3	0.8	0.5	0.8	0.1
Total	99.71	99.74	99.7	99.71	99.67	99.7	99.72	99.72	99.73	99.7	99.7	99.73	99.72	99.71	99.72
Trace elements (ppm)															
Rb	28.1	24.5	27.1	16.2	33	30.9	13.8	13.8	16.6	38.9	62.9	10.1	21.6	38.5	12.7
Ba	258	201	298	102	188	329	145	143	148	238	343	65	113	202	97
Cs	0.8	1.3	1.3	1.2	1.4	0.5	1.1	1.8	0.6	1.4	3	0.9	2.3	2.2	1.3
Sr	212.1	255	259.5	187.1	152.6	237.3	168.4	156.3	166	183.7	176.7	126.7	138.5	186	132.2
Pb	2.8	2.2	5.6	1	4.2	2.6	1.8	1.6	1.3	1.3	2.3	1	2	1.6	1.5
Th	2.9	1.2	3.4	0.9	3.9	2.3	1.9	1.5	1.8	2.9	4.2	1	2	2.6	1.7
U	0.6	0.5	1	0.3	1.3	0.6	0.4	0.4	0.4	0.8	1.2	0.3	0.7	0.6	0.5
Sc	33	29	35	32	40	38	45	39	37	39	34	39	40	35	41
V	317	194	266	281	461	310	316	294	282	324	276	250	359	293	341
Cr	34.21	68.42	68.42	68.42	34.21	34.21	68.42	102.63	102.63	34.21	34.21	171.05	68.42	68.42	136.84
Co	43.7	55.7	51.2	53.6	49.5	56	54.1	56.6	56.4	53.6	51.9	48.1	47.3	55	52.8
Ni	89	126	54	177	60	60	87	119	125	45	59	159	93	80	110
Y	31.7	23.8	442.2	21.4	44.6	37	23.5	23.7	27.2	40.3	51.5	16.6	29.5	35	27.5
Zr	140.2	103.4	228.1	105.9	202.1	176.2	79.4	84	109.1	197.8	285.9	53.8	99.2	167	92.2
Nb	8.2	5.1	12.3	6.9	13.6	9.6	4.7	4.3	5.6	10.6	16.6	3.1	5.8	8.8	5.1
Hf	3.8	3	6	2.7	5.3	4.5	2.2	2.5	2.9	4.9	7.6	1.6	3.1	4.6	2.6
Ta	0.5	0.3	0.8	0.4	0.9	0.6	0.3	0.3	0.4	0.7	1.1	0.2	0.4	0.5	0.3
La	17.9	10.6	22.5	9.2	18.9	18.1	9.3	9	11.2	21.3	32.7	5.5	9.4	18.2	8.2
Ce	39.9	24.7	52.2	23	46.7	40.7	20.4	20.8	25.7	48	74.3	12.7	22.5	40.8	20
Pr	5.1	3.21	6.53	3.04	5.83	5.43	2.79	2.81	3.42	6.21	9.17	1.74	3.06	5.28	2.77
Nd	21.2	14.5	29	13.7	26.9	23.2	12.3	13.5	15.2	27.7	39.1	8	14	23.5	13.9
Sm	4.86	3.35	6.33	3.45	6.72	5.29	3.14	3.18	3.71	5.89	7.82	2.03	3.63	5.13	3.35
Eu	1.55	1.21	1.81	1.32	2.03	1.62	1.09	1.09	1.21	1.75	2.15	0.79	1.19	1.57	1.15
Gd	5.58	3.89	7.14	4.05	7.83	5.88	3.63	3.8	4.19	6.53	8.43	2.63	4.52	5.71	4.2
Tb	0.94	0.7	1.26	0.71	1.4	1.04	0.68	0.67	0.77	1.17	1.48	0.48	0.81	1.02	0.77
Dy	5.57	4.18	7.46	4.14	8.37	6.35	4.15	4.23	4.81	6.95	8.65	2.94	4.94	5.94	4.68
Ho	1.15	0.84	1.59	0.81	1.75	1.31	0.85	0.89	0.94	1.46	1.83	0.6	1.04	1.26	1
Er	3.35	2.59	4.61	2.41	5.18	3.93	2.6	2.48	2.93	4.43	5.32	1.76	3.09	3.7	2.96
Tm	0.47	0.39	0.69	0.36	0.75	0.58	0.39	0.38	0.43	0.66	0.81	0.28	0.47	0.56	0.44
Yb	3.07	2.52	4.56	2.27	5.14	3.64	2.43	2.46	2.69	4.16	5.09	1.69	2.94	3.54	2.79
Lu	0.45	0.37	0.65	0.35	0.74	0.55	0.36	0.36	0.4	0.63	0.78	0.25	0.45	0.54	0.42

Appendix 1. Major and Trace element ICP-Ms analyses

Sample	BCD5-29	BCD5-30	BCD5-31	BCD5-32	BCD5-33	BCD5-34a	BCD5-34b	BCD5-35	BCD5-36	BCD5-37	BCD5-38	BCD5-54	BCD5-55	BCD5-78	BCD8-14
Major elements (wt%)															
SiO_2	49.36	49.53	47.68	51.34	48.98	50.03	49.91	50.58	49.24	49.59	49.4	49.34	49.58	49.73	48.57
Al_2O_3	16.46	15.81	15.22	13.58	12.48	12.91	12.73	13.74	13.46	14.5	15.49	16.7	16.37	13.12	11.22
Fe_2O_3	10.36	12.2	11.84	13.19	17.51	17.16	17.3	15.37	14.51	13.29	13.39	13.25	13.97	15.96	20.14
MgO	8.24	5.86	7.89	5.87	5.03	4.54	4.67	5.08	6.48	7.27	6.76	4.84	4.48	5.65	4.18
CaO	11.6	10.91	10.49	10.08	9.24	8.61	8.63	8.99	10.45	10.55	9.92	10.01	9.48	9.57	8.28
Na_2O	1.79	2.5	2.29	2.09	2.16	2.52	2.46	2.51	2.09	2.21	2.61	2.64	2.84	2.19	2.18
K_2O	0.29	0.56	0.62	0.57	0.8	1.42	1.38	1.14	0.48	0.32	0.59	0.77	0.86	0.75	1.14
TiO_2	0.77	1.13	1.09	1.34	2.47	2.41	2.41	1.85	1.62	1.15	1.16	1.57	1.72	2.03	3.01
P_2O_5	0.08	0.17	0.13	0.15	0.28	0.47	0.48	0.35	0.16	0.12	0.2	0.21	0.22	0.25	0.45
MnO	0.16	0.17	0.15	0.19	0.23	0.2	0.2	0.19	0.21	0.19	0.18	0.18	0.18	0.21	0.25
LOI	0.6	0.9	2.2	1.3	0.5	-0.6	-0.5	-0.1	1	0.5	0	0.2	0	0.2	0.2
Total	99.75	99.76	99.7	99.73	99.68	99.68	99.7	99.72	99.71	99.74	99.74	99.74	99.74	99.69	99.61
Trace elements (ppm)															
Rb	15.1	18.2	33.4	27.7	44.4	56.2	57.1	46.7	19.5	7.7	17.1	24	26.8	26.9	52.1
Ba	67	175	192	128	189	324	312	263	101	97	188	195	214	199	251
Cs	1.2	1.4	0.5	1.4	13	2.8	2.9	2.2	0.7	0.5	1.2	0.5	0.6	1.6	2.1
Sr	144.5	238	248.2	129.7	139.6	165.8	166.6	182.3	169	210.6	215.4	181.8	174.1	143.9	182.8
Pb	1	0.8	1	2.4	2.8	2.1	2	1.5	0.9	1.3	0.6	2.5	3	3.4	5.9
Th	0.7	0.8	0.6	2.9	4.4	4.4	4	3.6	1	0.5	1	3.5	3.7	4.3	6.5
U	0.2	0.3	0.1	0.7	1.3	1.2	1.2	1	0.3	0.2	0.3	0.8	0.8	1.2	1.9
Sc	36	35	30	43	44	37	37	34	45	37	32	32	32	42	43
V	236	224	237	349	460	339	341	294	342	266	209	308	316	370	453
Cr	136.84	68.42	205.26	34.21	34.21	34.21	34.21	34.21	68.42	102.63	68.42	68.42	34.21	68.42	34.21
Co	45.8	53.4	62.6	44.1	48.9	51.2	52.6	54	50.5	57.4	57	41.7	41.3	51.8	57.9
Ni	136	54	285	55	53	50	64	68	70	139	108	67	55	74	44
Y	14.7	20	19.8	29.5	49.3	48.3	47.8	38.5	26.1	18.4	22	30.9	31.5	37.5	62.3
Zr	46.5	74.2	72.6	105.8	193.2	266.8	264	221.8	102.4	66	90.9	143	145.2	164.9	292.7
Nb	2.4	3.6	3	6.3	13.6	15.2	15.4	13	7.8	3.8	4.6	8.3	8.8	10.6	18.5
Hf	1.3	2.2	2.1	3	5.3	6.9	7.4	5.8	3	2	2.6	4	4.2	4.6	7.6
Ta	0.1	0.3	0.2	0.4	0.9	0.9	0.9	0.8	0.5	0.2	0.3	0.5	0.6	0.7	1.3
La	4.7	8.2	6.7	11	18.9	30.5	29.7	24.8	8.7	6.3	10	15.4	16.7	17.2	27
Ce	10.7	19.1	15.7	25.9	44.9	68.9	67.1	56.7	22.3	15.8	23.3	35.7	37.6	40.1	64.7
Pr	1.5	2.55	2.21	3.42	5.97	8.52	8.3	6.83	3.04	2.2	2.95	4.41	4.71	5.12	8.22
Nd	7.1	12.5	11.1	16.3	27.7	37.4	35.7	28.9	14.5	10.4	13.4	19.9	20.6	23.3	38.4
Sm	1.86	2.77	2.73	3.95	6.66	7.75	7.66	6.11	3.77	2.77	3.15	4.81	4.96	5.69	9.4
Eu	0.71	1.08	1.02	1.25	2.02	2.04	2.06	1.73	1.28	1.04	1.13	1.51	1.57	1.76	2.68
Gd	2.31	3.22	3.2	4.67	8.02	8.18	8.28	6.5	4.58	3.16	3.64	5.53	5.68	6.59	11.05
Tb	0.41	0.58	0.59	0.87	1.43	1.46	1.45	1.16	0.81	0.59	0.66	0.97	1.01	1.2	1.98
Dy	2.58	3.49	3.56	5.29	8.8	8.42	8.57	6.88	4.64	3.33	3.98	5.66	6.13	6.91	11.66
Ho	0.54	0.74	0.75	1.1	1.83	1.81	1.76	1.42	1.03	0.7	0.83	1.2	1.22	1.5	2.46
Er	1.52	2.03	2.19	3.12	5.09	4.98	5.24	4.04	2.97	1.94	2.45	3.48	3.55	4.35	6.98
Tm	0.25	0.32	0.33	0.48	0.77	0.75	0.76	0.64	0.44	0.28	0.37	0.52	0.53	0.66	1.08
Yb	1.5	2.15	2.01	3.05	4.95	5.01	4.86	4.02	2.71	1.91	2.28	3.24	3.42	4.1	6.83
Lu	0.23	0.31	0.3	0.47	0.76	0.76	0.75	0.61	0.42	0.28	0.35	0.5	0.52	0.64	1.03

Appendix 2. Sample location map

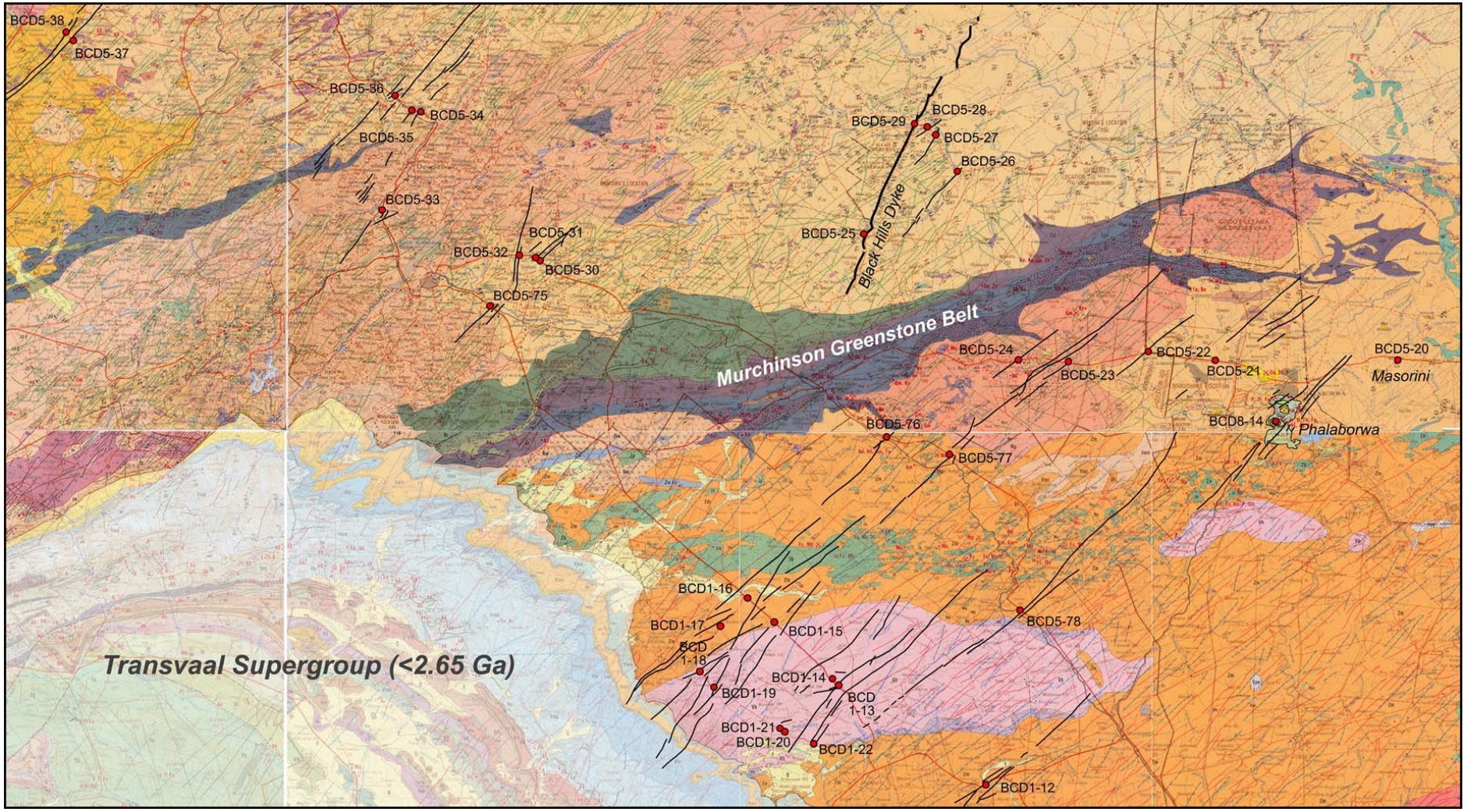

Appendix 3. Results from the correspondence analysis for the samples and certain chemical elements

Sample	F1	F2	F3
BCD1-12	0,06	-0,04	-0,01
BCD1-13	0,16	0,24	0,04
BCD1-15	0,15	-0,1	0,04
BCD1-17	-0,18	0,35	-0,02
BCD1-18	-0,27	-0,19	-0,12
BCD1-19	0,13	-0,05	-0,04
BCD1-21	-0,17	0,09	-0,04
BCD1-22	-0,17	0,12	-0,06
BCD5-21	-0,14	0,11	-0,04
BCD5-22	-0,02	-0,15	0,01
BCD5-23	0,23	-0,22	0,16
BCD5-25	-0,27	0,23	0,05
BCD5-26	-0,27	0,02	-0,03
BCD5-27	-0,02	-0,07	0,04
BCD5-28	-0,31	0,05	-0,03
BCD5-29	-0,26	0,24	0,02
BCD5-30	0,09	0,2	0,04
BCD5-31	0,04	0,53	-0,1
BCD5-32	-0,22	-0,05	0
BCD5-33	-0,28	-0,23	-0,13
BCD5-34A	0,17	-0,2	0,15
BCD5-34B	0,16	-0,19	0,15
BCD5-35	0,15	-0,14	0,16
BCD5-36	-0,28	0,01	-0,04
BCD5-37	-0,17	0,24	0,02
BCD5-38	0,13	0,24	0,06
BCD5-54	-0,09	-0,04	-0,06
BCD5-55	-0,1	-0,08	-0,1
BCD5-78	-0,14	-0,13	-0,02
BCD8-14	-0,16	-0,25	-0,04

Element	F1	F2	F3
Si	-0,07	0,18	0,15
Al	-0,08	0,18	0,04
Fe	-0,1	0,03	0,07
Mn	-0,12	0,1	0,1
Mg	-0,23	0,48	0,3
Ca	-0,17	0,25	0,14
Na	0,06	0,1	0,12
K	0,18	-0,1	0,08
Ti	-0,06	-0,15	0,05
P	0,13	-0,22	0,2
Cr	-0,25	0,89	0,53
Sc	-0,21	0,12	0,08
Ba	0,44	-0,05	-0,15
Co	-0,11	0,22	0,11
Cs	-0,26	-0,35	-0,1
Ga	-0,06	0,07	0,06
Hf	0,07	-0,22	0,14
Nb	0,02	-0,28	0,17
Rb	0,13	-0,18	0,03
Sr	0,16	0,21	0,02
Ta	0,02	-0,3	0,18
Th	-0,01	-0,32	0,12
U	-0,01	-0,33	0,15
V	-0,23	-0,01	-0,01
Zr	0,08	-0,25	0,13
Y	-0,04	-0,17	0,1
La	0,17	-0,22	0,23
Ce	0,13	-0,21	0,21
Pr	0,11	-0,19	0,22
Nd	0,09	-0,17	0,21
Sm	0,01	-0,15	0,17
Eu	-0,02	-0,07	0,15
Gd	-0,02	-0,15	0,14
Tb	-0,04	-0,16	0,12
Dy	-0,05	-0,16	0,1
Ho	-0,05	-0,17	0,1
Er	-0,05	-0,17	0,09
Tm	-0,05	-0,17	0,09
Yb	-0,05	-0,18	0,08
Lu	-0,06	-0,18	0,09
Cu	-0,35	-0,1	-0,2
Pb	0,29	-0,1	-0,07
Zn	-0,1	-0,08	-0,09
Ni	0,04	0,73	-0,03

	F1	F2	F3
Largest contribution to inertia (in %):	43,16	26,97	10,73

Appendix 4. Sample description of the samples used for the geochemistry

Sample	Longitude	Latitude	Matrix grain size	Present minerals	Exposure	Description
BCD1-12	30.79738	24.40592	medium to coarse	Plagioclase, Pyroxene	Road cut	Dyke
BCD1-13	30.62963	24.29228	medium to coarse	Plagioclase, Pyroxene, Olivine	Road outcrop	Dyke
BCD1-15	30.55603	24.22053	fine	Plagioclase, Pyroxene	River outcrop	Fractured dyke
BCD1-17	30.49459	24.22503	fine to medium	Plagioclase, Pyroxene, Olivine	Dirt Raod „pavement“	Dyke
BCD1-18	30.47125	24.27669	fine to medium	Plagioclase, Pyroxene	Road cut	Slightly amph. dyke
BCD1-19	30.48741	24.29496	fine	Plagioclase, Pyroxene	Road cut	Fresh dyke
BCD1-21	30.56809	24.34537	fine to medium	Plagioclase, Pyroxene	Large boulders	Dyke
BCD1-22	30.60133	24.35910	medium	Plagioclase, Pyroxene, Olivine	Large boulders	Dolerite dyke
BCD5-21	31.05923	23.92204	medium to coarse	Plagioclase, Pyroxene, Olivine	Boulders	Dolerite dyke
BCD5-22	30.98279	23.91204	medium	Plagioclase, Pyroxene	Solid outcrop	Dolerite dyke
BCD5-23	30.89176	23.92318	medium to coarse	Plagioclase, Pyroxene	River outcrop	Black Hills dyke
BCD5-25	30.65823	23.77793	coarse	Plagioclase, Pyroxene	Distinct ridge	Fresh dyke
BCD5-26	30.76503	23.70650	medium to coarse	Plagioclase, Pyroxene	Boulders	Dyke
BCD5-27	30.74012	23.66452	medium	Plagioclase, Pyroxene	Boulders	Dyke
BCD5-28	30.73052	23.65573	medium	Plagioclase, Pyroxene, Olivine	Boulders	Dyke
BCD5-29	30.71606	23.65198	coarse	Plagioclase, Pyroxene	Distinct ridge	Black Hills dyke
BCD5-30	30.28909	23.80821	fine	Plagioclase, Pyroxene, Olivine	Boulders	Dyke
BCD5-31	30.28401	23.80453	fine to medium	Plagioclase, Pyroxene, Olivine	Boulders	Slightly altered dyke
BCD5-32	30.26548	23.80206	medium	Plagioclase, Pyroxene	Solid outcrop	Fresh dyke
BCD5-33	30.10876	23.75056	fine	Plagioclase, Pyroxene	River outcrop	Fresh dyke
BCD5-34a	30.15317	23.63859	medium	Plagioclase, Pyroxene	Boulders	Fresh dyke
BCD5-34b	30.15317	23.63859	medium	Plagioclase, Pyroxene	Boulders	Fresh dyke
BCD5-35	30.14280	23.63654	coarse	Plagioclase, Pyroxene	Boulders	Fresh dyke
BCD5-36	30.12409	23.61985	fine to medium	Plagioclase, Pyroxene	Boulders	Dyke
BCD5-37	29.75694	23.55721	medium	Plagioclase, Pyroxene, Olivine	Boulders	Fresh dyke
BCD5-38	29.74869	23.54747	medium	Plagioclase, Pyroxene, Olivine	Boulders	Fresh dyke
BCD5-54	27.79895	20.75183	medium to coarse	Plagioclase, Pyroxene, Olivine	Boulders	Dolerite sill, slightly altered
BCD5-55	27.80394	20.76345	coarse	Plagioclase, Pyroxene, Olivine	River outcrop	Dolerite sill
BCD5-78	30.83629	24.20702	coarse	Plagioclase, Pyroxene	Boulders	Fresh dolerite dyke
BCD8-14	31.12555	23.98722	medium	Plagioclase, Pyroxene	Phalaborwa mine	Sample from a mine

Tidigare skrifter i serien ”Examensarbeten i Geologi vid Lunds Universitet”:

218. Ohlsson, Erika, 2007: Classification of stony meteorites from north-west Africa and the Dhofar desert region in Oman.
219. Åkesson, Maria, 2008: Mud volcanoes - a review. (15 hskp)
220. Randsalu, Linda, 2008: Holocene relative sea-level changes in the Tasiusaq area, southern Greenland, with focus on the Ta1 and Ta3 basins. (30 hskp)
221. Fredh, Daniel, 2008: Holocene relative sea-level changes in the Tasiusaq area, southern Greenland, with focus on the Ta4 basin. (30 hskp)
222. Anjar, Johanna, 2008: A sedimentological and stratigraphical study of Weichselian sediments in the Tvärkroken gravel pit, Idre, west-central Sweden. (30 hskp)
223. Stefanowicz, Sissa, 2008: Palyno-stratigraphy and palaeoclimatic analysis of the Lower - Middle Jurassic (Pliens-bachian - Bathonian) of the Inner Hebrides, NW Scotland. (15 hskp)
224. Holm, Sanna, 2008: Variations in impactor flux to the Moon and Earth after 3.85 Ga. (15 hskp)
225. Bjärnborg, Karolina, 2008: Internal structures in detrital zircons from Hamrånge: a study of cathodolumine-scence and back-scattered electron images. (15 hskp)
226. Noresten, Barbro, 2008: A reconstruction of subglacial processes based on a classification of erosional forms at Ramsvikslandet, SW Sweden. (30 hskp)
227. Mehlqvist, Kristina, 2008: En mellanjuras-sisk flora från Bagå-formationen, Bornholm. (15 hskp)
228. Lindvall, Hanna, 2008: Kortvariga effekter av tefranedfall i lakustrin och terrestrisk miljö. (15 hskp)
229. Löfroth, Elin, 2008: Are solar activity and cosmic rays important factors behind climate change? (15 hskp)
230. Damberg, Lisa, 2008: Pyrit som källa för spårämnen – kalkstenar från övre och mellersta Danien, Skåne. (15 hskp)
331. Cegrell, Miriam & Mårtensson, Jimmy, 2008: Resistivity and IP measurements at the Bolmen Tunnel and Ådalsbanan, Sweden. (30 hskp)
232. Vang, Ina, 2008: Skarn minerals and geological structures at Kalkheia, Kristiansand, southern Norway. (15 hskp)
233. Arvidsson, Kristina, 2008: Vegetationen i Skandinavien under Eem och Weichsel samt fallstudie i submoräna organiska avlagringar från Nybygget, Småland. (15 hskp)
234. Persson, Jonas, 2008: An environmental magnetic study of a marine sediment core from Disko Bugt, West Greenland: implications for ocean current variability. (30 hskp)
235. Holm, Sanna, 2008: Titanium- and chromium-rich opaque minerals in condensed sediments: chondritic, lunar and terrestrial origins. (30 hskp)
236. Bohlin, Erik & Landen, Ludvig, 2008: Geofysiska mätmetoder för prospektering till ballastmaterial. (30 hskp)
237. Brodén, Olof, 2008: Primär och sekundär migration av hydrokarboner. (15 hskp)
238. Bergman, Bo, 2009: Geofysiska analyser (stångslingram, CVES och IP) av lagerföljd och lakvattenrörelser vid Albäcksdeponin, Trelleborg. (30 hskp)
239. Mehlqvist, Kristina, 2009: The spore record of early land plants from upper Silurian strata in Klinta 1 well, Skåne, Sweden. (45 hskp)
239. Mehlqvist, Kristina, 2009: The spore record of early land plants from upper Silurian strata in Klinta 1 well, Skåne, Sweden. (45 hskp)
240. Bjärnborg, Karolina, 2009: The copper sulphide mineralization of the Zinkgruvan deposit, Bergslagen, Sweden. (45 hskp)
241. Stenberg, Li, 2009: Historiska kartor som hjälp vid jordartsgeologisk kartering – en pilotstudie från Vångs by i Blekinge. (15 hskp)
242. Nilsson, Mimmi, 2009: Robust U-Pb baddeleyite ages of mafic dykes and intrusions in southern West Greenland: constraints on the coherency of crustal blocks of the North Atlantic Craton. (30 hskp)
243. Hult, Elin, 2009: Oligocene to middle Miocene sediments from ODP leg 159, site 959 offshore Ivory Coast, equatorial West Africa. (15 hskp)
244. Olsson, Håkan, 2009: Climate archives and

the Late Ordovician Boda Event. (15 hskp)

245. Wollein Waldetoft, Kristofer, 2009: Svekofennisk granit från olika metamorfa miljöer. (15 hskp)
246. Månsby, Urban, 2009: Late Cretaceous coprolites from the Kristianstad Basin, southern Sweden. (15 hskp)
247. MacGimpsey, I., 2008: Petroleum Geology of the Barents Sea. (15 hskp)
248. Jäckel, O., 2009: Comparison between two sediment X-ray Fluorescence records of the Late Holocene from Disko Bugt, West Greenland; Paleoclimatic and methodological implications. (45 hskp)
249. Andersen, Christine, 2009: The mineral composition of the Burkland Cu-sulphide deposit at Zinkgruvan, Sweden – a supplementary study. (15 hskp)
250. Riebe, My, 2009: Spinel group minerals in carbonaceous and ordinary chondrites. (15 hskp)
251. Nilsson, Filip, 2009: Föroreningsspridning och geologi vid Filborna i Helsingborg. (30 hskp)
252. Peetz, Romina, 2009: A geochemical characterization of the lower part of the Miocene shield-building lavas on Gran Canaria. (45 hskp)
253. Åkesson, Maria, 2010: Mass movements as contamination carriers in surface water systems – Swedish experiences and risks.
254. Löfroth, Elin, 2010: A Greenland ice core perspective on the dating of the Late Bronze Age Santorini eruption. (45 hskp)
255. Ellingsgaard, Óluva, 2009: Formation Evaluation of Interlava Volcaniclastic Rocks from the Faroe Islands and the Faroe-Shetland Basin. (45 hskp)
256. Arvidsson, Kristina, 2010: Geophysical and hydrogeological survey in a part of the Nhandugue River valley, Gorongosa National Park, Mozambique. (45 hskp)
257. Gren, Johan, 2010: Osteo-histology of Mesozoic marine tetrapods – implications for longevity, growth strategies and growth rates. (15 hskp)
258. Syversen, Fredrikke, 2010: Late Jurassic deposits in the Troll field. (15 hskp)
259. Andersson, Pontus, 2010: Hydrogeological investigation for the PEGASUS project, southern Skåne, Sweden. (30 hskp)
260. Noor, Amir, 2010: Upper Ordovician through lowermost Silurian stratigraphy and facies of the Borenshult-1 core, Östergötland, Sweden. (45 hskp)
261. Lewerentz, Alexander, 2010: On the occurrence of baddeleyite in zircon in silica-saturated rocks. (15 hskp)
262. Eriksson, Magnus, 2010: The Ordovician Orthoceratite Limestone and the Blommiga Bladet hardground complex at Horns Udde, Öland. (15 hskp)
263. Lindskog, Anders, 2010: From red to grey and back again: A detailed study of the lower Kundan (Middle Ordovician) 'Täljsten' interval and its enclosing strata in Västergötland, Sweden. (15 hskp)
264. Rääf, Rebecka, 2010: Changes in beyrichiid ostracode faunas during the Late Silurian Lau Event on Gotland, Sweden. (30 hskp)
265. Petersson, Andreas, 2010: Zircon U-Pb, Hf and O isotope constraints on the growth versus recycling of continental crust in the Grenville orogen, Ohio, USA. (45 hskp)
266. Stenberg, Li, 2010: Geophysical and hydrogeological survey in a part of the Nhandugue River valley, Gorongosa National Park, Mozambique – Area 1 and 2. (45 hskp)
267. Andersen, Christine, 2010: Controls of seafloor depth on hydrothermal vent temperatures - prediction, observation & 2D finite element modeling. (45 hskp)
268. März, Nadine, 2010: When did the Kalahari craton form? Constraints from baddeleyite U-Pb geochronology and geo-chemistry of mafic intrusions in the Kaapvaal and Zimbabwe cratons. (45 hskp)

LUNDS UNIVERSITET

Geologiska enheten
Institutionen för geo- och ekosystemvetenskaper
Sölvegatan 12, 223 62 Lund